EMPIRICAL ANALYSIS OF CUTTING FORCE CONSTANTS IN MICRO END MILLING OPERATIONS

A Thesis
Presented to
The Academic Faculty

by

Glynn Newby

In Partial Fulfillment
of the Requirements for the Degree
Master of Science in Mechanical Engineering

George W. Woodruff School of Mechanical Engineering
Georgia Institute of Technology
August 5, 2005

EMPIRICAL ANALYSIS OF CUTTING FORCE CONSTANTS IN MICRO END MILLING OPERATIONS

Approved by:

Dr. Steven Y. Liang, Committee Chair
School of Mechanical Engineering
Georgia Institute of Technology

Dr. Min Zhou
School of Mechanical Engineering
Georgia Institute of Technology

Dr. Shreyes N. Melkote
School of Mechanical Engineering
Georgia Institute of Technology

Date Approved: August 5, 2005

To my Lord and Savior Jesus Christ. Thanks for the Holy playbook.

ACKNOWLEDGEMENTS

The authors would like to take this opportunity to thank the engineers and scientists at PMC Inc. of Taiwan. The construction of the micro milling machine used in this research was developed as a joint effort between PMC and the PMRC (Precision Machining Research Consortium) at Georgia Tech. Any opinions findings and conclusions or recommendations are those of the authors and do not necessarily reflect the views of PMC.

TABLE OF CONTENTS

LIST OF TABLES

LIST OF FIGURES

LIST OF SYMBOLS OR ABBREVIATIONS

α	cutter helical angle.
$\beta - r - h$	angular, radial, and axial position variables for cutting point in cylindrical coordinate system.
β_a	angular range of axial immersion of each flute within axial depth of cut.
β_p	angular spacing between two adjacent flutes, 2π/N.
c	workpiece recess.
CEMO	conventional end milling operation.
d_a	axial depth of cut.
δ	computing angle.
D	cutter diameter.
d_r	radial depth of cut.
η_a	β_a/β_p.
η_c	c/D.
η_r	d_r/D.
f_c	computing feed rate.
f	feed rate.
F_r	radial cutting force.
F_t	tangential cutting force.
F_x	cutting force in feed direction.
F_y	cutting force perpendicular to feed direction.
K_r	ratio of radial to tangential cutting force.
K_t	average tangential cutting pressure constant.
N	number of cutter flutes.
R	cutter radius.
MEMO	micro end milling operation.
n	spindle speed.
ϕ	cutter angular displacement.
$\theta(\phi, \beta)$	cutting point angular position in the work.

θ_{1r}	entry angle.
θ_{2r}	exit angle.
θ_{rr}	radial cutting range from cutting configuration.
$t_c(\theta), t_c(\theta, \beta)$	uncut chip thickness.
$\bar{t}_c$	average chip thickness.
τ_r	feed per tooth per cutter radius ratio.
t_x	feed per tooth.
ω	spindle circle frequency (1/sec).
$\mathbf{w}(\theta)$	cutting window function for the radial cutting configuration.
Ω	spindle frequency.
XYZ	the work coordinate system.

SUMMARY

The development of miniaturized technologies has become a global phenomenon that continues to make broad impacts across a broad range of applications that encompasses many diverse fields and industries including telecommunications, portable consumer electronics, defense, and biomedical. Subsequently this trend has caused an increasing interest in the issues involved in the design, development, operation and analysis of equipment and processes of manufacturing micro components.

One technology used to create these miniaturized components is micro end milling. The cutting forces of the micro end milling process provide vital information for the design, modeling, and control of the machining process. To gain an understanding of forces in micro end milling operations, a model for average chip thickness in micro end milling is derived and the differences between conventional end milling and micro end milling operations are enumerated. From the experimental results, empirical models for specific cutting pressure constants were derived and compared to the generally accepted forms for conventional end milling operations. These models provide a tool for the estimation of cutting forces in micro end milling.

CHAPTER I

INTRODUCTION

The objective of this research is to provide an empirical model for further understanding of the cutting force system of the micro end milling process. This objective is achieved through the experimental determination of an equation to represent cutting coefficients in micro end milling operations. Additionally, this objective is achieved through the use of closed form relationships between cutting forces and cutting parameters in the micro end milling regime such as feed rate, depth of cut, and cutter geometry. Such a model will provide a better tool for the analysis and control of the micro end milling process.

1.1 Motivation: A case study in micro end milling

The development of miniaturized technologies has become a global phenomenon that continues to make marked impacts across a broad application domain that encompasses many diverse fields and industries, including telecommunications, portable consumer electronics, defense, and biomedical. For example, computers such as the ENIAC (electronic numerical integrator and computer) once filled large rooms, but modern computers contain greater processing power and can fit under a desk or on a lap. As the global trend toward the increased integration of miniaturized technology into society gains momentum, more and more attention is being paid to the issues involved in the design, development, operation, and analysis of the equipment and processes of manufacturing micro components. Currently, common techniques utilized in the fabrication of micro-components are based on the techniques developed for the silicon wafer processing industry that are based primarily on optical lithography. Unfortunately these processes are cost effective only in large volume and are limited to production of simple planar geometries in a narrow range of material [22]. Nontraditional fabrication methods, such as focused ion beam machining, laser machining, and electrodischarge machining, are capable of producing high-precision micro-components,

but have limited potential as mass production techniques due to the high initial cost, poor productivity, and limited material selection [27]. Research into the development of flexible, effective production technologies for micro components has therefore intensified.

The increased research and development of nanotechnologies requires the development of integration and packaging structures that provide the interface between the nanotechnologies and the macro world. This further increases the demand for more effective production methods for micro and mesoscale components with complex three dimensional forms in a broad range of material. Therefore the development of precision micro-mechanical machining processes including turning, milling, and drilling, has become an attractive alternative and active area of exploration. Research into the development of flexible, effective production technologies for micro components has therefore intensified.

The authors recognized this trend of miniaturization and the need for advanced technologies in this area. Producing micro components and features on conventionally sized machine tools seemed counterintuitive. Therefore, a micro machining center was designed in order to analyze the performance increase, reduction of power consumption, reduction of waste, and improvement in finish quality that was anticipated by miniaturization of a milling machine. The micro machining center was constructed a result of a collaboration between Georgia Tech and PMC Inc. and is now being used for research and analysis of the machining on the micro scale.

During the course of this research the authors were presented with an opportunity to create a micro-scale feature for GE Research. At that time there was no model available to estimate cutting forces generated during the micro end milling operation. The feature, as illustrated in Figure 1, was a sinusoidal trough. The trough had a length of 500 microns, a width of 100 microns, and the depth of the trough was on the order of 50 microns. The sinusoidal surface at the bottom of the trough had a width of 25 microns. Shallow depths of cut and a slow feed of 0.0635 mm/min(0.0025 in/min) were used because of the desire not to break the micro end mill, having only a 10 micron diameter. As a result of these machining parameters the micro feature took 20 hours to machine. That time does not include the setup time, which was also a considerable amount of time due to the lack of

tactile feed back and other complexities operating of the micro end milling machine.

If a model for approximating forces in micro end milling operations had been available, the machining time could have been drastically reduced. Such a model would enable machinists to anticipate the forces experienced by the diminutive end mill and select appropriately aggressive machining parameters in order to maximize material removal and productivity, while minimizing the potential of tool failure. This case study exemplifies the need for research in the area of the cutting process of micro end milling operations.

1.2 Previous Work

The cutting process of conventional end milling operations has been studied and understood since the early 20^{th} century. Martellotti [25] [26] analyzed the kinematics of the milling process in detail and determined an expression for the basic chip thickness that has been used by many researchers. The chip thickness, along with tool geometry, tool material properties, and the workpiece properties determine the forces that are generated during the cutting operations. An empirical model proposed by Koenigsbsber and Sabberwal [19] for the tangential cutting force and a model by Tlusty [37] for the radial cutting force have been shown to accurately predict the cutting forces in conventional end milling operations and are commonly used to relate the chip thickness to the cutting force [45]. This body of knowledge has enabled researchers to relate tangential and radial components of cutting force to the average chip thickness through two cutting constants, K_t and K_r. K_t is the tangential specific cutting pressure constant and K_r is the ratio of the local radial cutting force to the tangential cutting force. Both cutting pressure constants are dependent on feed, tool edge geometry, and the workpiece material, and are generally obtained from experiments.

In recent years several industries have experienced a trend of miniaturization. As a result, research into the development of flexible and effective production technologies for micro components has intensified. Nontraditional fabrication methods, such as focused ion beam machining, laser machining, and electrodischarge machining, are capable of producing high precision micro-components, but have limited potential as mass production techniques

due to the high initial cost, poor productivity, and limited material selection [27]. Therefore, the development of precision micro-mechanical machining processes including turning, milling, and drilling, has become an active research area. Prior research into micro-milling has established that it is an attractive alternative for micro-component manufacturing due to the inherent flexibility of the process in its ability to produce complex three-dimensional features.

Initial explorations into micro end milling operations focused on the cutting tool itself. In one of the earliest contributions to the field of micro machining, Vasile et al. [38] fabricated 25 micron diameter steel milling tools using a focused ion beam and utilized these tools on a purpose-built precision milling machine to machine pairs of trenches 24 microns wide, 26 microns deep and 2.3mm long. Note that although the tools were miniaturized, the machine tools used in these explorations into micro end milling were still of conventional size.

The next phase of research in micro end milling focused on reducing the size of the machine tool itself. Lu et al. [24] designed and analyzed a micro lathe turning system. The micro lathe developed had a maximum dimension of length 200mm and was built from commercially available products. The spindle of the lathe had a maximum speed of 15,000rpm and the workpiece material was 0.3mm in diameter. The material removal was facilitated by a diamond single point tool, and the process was monitored using an optical microscope. The lathe was successful in creating micro components such as a screw of 120 micron diameter, but the achievable surface finish was not substantially better than conventional lathes. Many other studies have revealed the ability of the micro-milling process to fabricate microcomponents [16] [39] [3] [34].

Despite this understanding of the cutting process at a macro scale and the advances in the process capabilities of micro machining, little research has been conducted to gain a fundamental understanding of the mechanisms of the micro-milling process. At the micro-scale there are differences in the process that can not be described by the simple scaling of the conventional end milling process. One of the differences at the micro-scale arises form the breakdown of the assumptions of homogeneity in the workpiece microstructure and of negligible edge radius effects. Chuzhoy et al. [9] [10] developed a microstructure-level

simulation model of heterogeneous materials, such as cast iron, to investigate machining behavior in micro milling. They reported that the variation of chip morphology and cutting forces is larger when cutting a multiphase material as compared to a single-phase material. Another difference between micro and conventional end milling operations is that as the size of a tool decreases, the sharpness of the tool cannot be improved proportionally due to limitations in the tool fabrication processes and the reduction in structural strength of the tool. As a result, the feed per tooth in micro-milling may be comparable to, or even less than, the cutting edge radius because of the required range of process parameters for stable machining. This decreases productivity in the name of preservation of the micro end mills. This is a negative effect of the miniaturization of the machining process and it is precisely this problem which is addressed in this research. The determination of cutting constants in micro end milling operations will allow for the maximum levels of productivity in the machining process.

1.3 Presented Approach

This thesis presents an analysis of cutting forces in micro end milling operations. The approach used in this thesis uses the fact that micro end milling operations traditionally have higher feed per tooth per radius of cutter ratios than in conventional end milling operations. The true trochoidial nature of the tool edge path is taken into consideration in the derivation of a chip thickness for micro end milling operations. Cutting experiments were conducted in the micro end milling regime and forces were recorded. These forces were then decomposed in order to present new empirical formulas for cutting pressure constants in micro end milling operations. These empirical equations for cutting constants are a tool that will aid in the understanding of friction and the prediction of forces in micro end milling operations.

CHAPTER II

KINEMATICS OF CHIP FORMING PROCESS

2.1 Introduction

Chip formation is a fundamental component of the milling process. This chip thickness depends on the trajectory and runout of the tool. These dependencies are described in the following subsections.

2.1.1 Chip thickness and tool trajectories in milling

Milling is a machining operation in which metal or other material is removed by bringing the workpiece into contact with a horizontally or vertically mounted cutter. This material removal can be physically observed by the formation of chips during the cutting process. The cutting parameters physically determine the trajectory of the tool. Furthermore, this trajectory determines the average thickness of the chips produced during the milling operation. As a result, this chip thickness has an impact upon the forces observed during milling.

There have been considerable efforts in research and experimentation throughout the 20^{th} century aiming at understanding the basics of the milling process, particularly the chip formation. Models have been proposed to explain the phenomena occurring when material is removed from the workpiece in the form of chips. Research of chip formation in metals had been carried out as far back as 1873, but fundamental theories and models seem to have appeared at the beginning of the 20^{th} century only [21]. Again, chip thickness is known to have a dependance upon the trajectory of the tool and traditionally the cutting points of the trajectory of conventional milling operations have been assumed to be circular. Martellotti[25][26] for the first time derived equations for the true tooth trajectories for peripheral milling of straight surfaces and showed that such a trajectory is a trochoid. It was then concluded that in conventional milling of straight surfaces the difference in

chip thickness calculations by either circular or trochoidial trajectories is negligible. You and Ehmann[43][44] developed similar tooth trajectories for face milling with ball nose and cutter. Subsequently, Spiewak[32][33] derived a more comprehensive model for cutting tooth trajectory by homogenous transformation of coordinate systems associated with the motion between the cutting tooth and workpiece in peripheral milling of straight surfaces. More recently, Li et al.[23] gave an improved method for estimation of undeformed chip thickness using true tooth trajectories which was based on a Taylor Series approximation.

The general chip thickness, t_c, for an active cutting point on a cutter without runout is dependent upon the trajectory of the tool. Martellotti[25][26] approximated this relationship as

$$t_c(\theta) = t_x \sin\theta \tag{1}$$

where t_c is instantaneous chip thickness, t_x is feed per tooth, and θ is the angular position of the tooth. This expression has been used for several decades because most milling tasks could be classified as having relatively low feed rates compared to the radius of the tool, and therefore the true trochoidial path could be neglected. More recently, Engin et al.[11][12] presented a generalized mathematical model of most helical end mills and inserted cutters used in industry. The end mill and insert geometries were modeled, and the cutting edge locations were defined mathematically. These models and the true kinematics of milling, including the structural vibrations of both cutter and workpiece, were used in predicting the chip thickness distribution along the cutting zone. It is shown in this study that the trochoidal nature of the trajectory can not be neglected in micro end milling.

2.1.2 Chip thickness and runout

A complete analysis of forces in milling requires the thorough analysis of the kinematics of chip load variation due to cutter runout. The first analysis of cutter runout effect on chip load for an end mill cutter is reported by Kline et al.[17] on the down milling operation. He showed that the chip thickness, average chip thickness and exit angle change as a result of cutter radial offset. A numerical algorithm is presented to calculate the chip thickness. An empirical equation for the average chip thickness, which is used for calculating the cutting

pressure constant, was given for down milling with a four flute cutter. A mechanistic milling force model was then presented which incorporated the revised chip thickness equation for the prediction of total milling forces. Modeling of radial and axial runout in a face milling cutter and their effect on tool wear were presented by Ber and Feldman[6][7]. Other researchers have also proposed models of the cutting forces in end milling and face milling with cutter runout[14][2]. All presented chip thickness expressions including the cutter runout effect. The effect of cutter runout is neglected in this study.

2.1.3 Chip thickness in micro end milling

Equation 1 for chip thickness is acceptable for conventional end milling operations. However, there are differences in the chip formation process on the micro scale. Kim et al.[16] developed an enhanced, static model for chip formation in micro milling processes that is able to describe the intermittence of the chip formation observed at low feeds per tooth due to the dominance of the minimum chip thickness effect. A key finding of this study is the identification of a local maximum in the radial thrust forces in the micro-milling process during the non-cutting regime, at feeds pert tooth that are on the order of the minimum chip thickness.

Volger et al.[39][40]examined the surface generation process in the micro end milling of both single-phase and multi-phase workpiece materials. A cutting force model for the micro endmilling process was developed which incorporated the minimum chip thickness concept in order to predict the effects of the cutter edge radius on the cutting forces. Bao and Tansel[4] developed and validated an analytical cutting force model for micro end milling operations with tool runout. Again, tool runout is neglected in this research.

In this work Section 2.2 explains the differences between conventional end milling operations and micro end milling operations. A new constant for the feed per tooth per radius of tool is proposed. Section 2.3 describes cutting points in the milling operation and Section 2.4 uses this representation in order to distinguish the chip thicknesses in conventional and micro end milling operations.

2.2 Definition of CEMO and MEMO

An initial observation of the micro end milling operation (MEMO) would lead one to believe that it is the same as conventional end milling operations (CEMO) with only differences in dimension. However, there are several key differences. In MEMO, aggressively higher feeds are usually selected in order to maintain acceptable levels of productivity. As a result, the tiny shaft of a micro tool is under a much higher level of stress than conventional tools and tool life can dramatically reduce. If cutting conditions are not appropriately selected, tools will break in seconds and, because of their small size, damage to the tool may go unnoticed and waste many hours of machining time.

In CEMO, the machine tool typically occupies a volume on the order of $3m^3(106ft^3)$, and each axis can have a range of travel of several meters. These machine tools are equipped with end mills that range in diameter from $3.175mm(1/8in)$ to $25.4mm(1in)$ and even larger effective diameters can be obtained by using cutter inserts. On the other hand, in MEMO, machine tools typically occupy a space on the order of $0.3m^3(1ft^3)$ or less. The travel of each axis is usually limited to tens of mm, and diameters of end mills used in MEMO typically range from $1.6mm(1/16in)$ to smaller than $0.0254mm(0.001in)$.

Again, in MEMO more aggressive feed rates are usually selected in order to maintain high levels of machining productivity. CEMO have feeds per tooth which are relatively low compared to the radius of the end mills. In MEMO, on the other hand, the feed per tooth is relatively high compared to the radius of the end mills. This feed per tooth per radius ratio is what distinguishes MEMO from CEMO. Bao and Tansel [3] propose that MEMO is defined as an end milling operation in which the feed per tooth per radius ratio is greater than 0.1, and that ratio is less than 0.1 for a CEMO. This convention is used in this research, and because the authors believe that this ratio will have such a large impact on the future of manufacturing technologies we propose a new constant for this ratio

$$\tau_r = \frac{t_x}{R}. \tag{2}$$

2.3 Position Representations of Cutting Points

The position representation model of cutting points developed by Wang [41] is used and represented in the following: To represent the geometry of active cutting edges a cylindrical coordinate system, $\beta - r - h$, is attached to the cutter as shown in Figure 5 (a). A point is termed active if it is located within the axial depth of cut and will engage in the cutting process. The h axis of the coordinate system is coincident with the axis of cutter rotation. The origin is typically specified as being located on the face of the end mill with positive h pointing to the end of the tool that is held by the chuck of the spindle. If a cutter has N flutes, there are N active cutting points at each axial position, h, within the axial depth of cut. The angular position of the cutting point at $h = 0$ on an arbitrarily chosen first flute is defined to be $\beta = 0$, and the β increases in the positive direction. Therefore the active cutting edge line geometry of the k^{th} flute on an N-flute end mill can be described as

$$h_k = \frac{R}{\tan\alpha}(\beta - (k-1)\beta_p), \quad k = 1, 2 \ldots \infty, \quad (k-1)\beta_p \leq \beta \leq (k-1)\beta_p + \beta_a \quad (3)$$

$$r_k = R$$

where β, r and h are the angular, radial and axial positions of each active cutting point, $\beta_p = \frac{2\pi}{N}$, the angular spacing for an N-flute cutter, and

$$\beta_a = \frac{d_a}{R}\tan\alpha \quad (4)$$

is the angular range of axial immersion of each cutter flute determined by the cutter radius, R, the axial depth of cut, d_a, and the cutter helical angle, α. A figure of the function h_k is shown in Figure 5 (b). The N-flute cutter is treated mathematically as an unfolded cutter with an infinite number of flutes. The flute number, k, ranges from 1 to ∞ and flute number $N + k$ is the same as flute number k. $h_k(\beta)$ is defined only within a range of β determined by the flute number k and β_a such that h_k is constrained between 0 and d_a. Only cutting points within that range of motion are actively engaged in the cutting process and are therefore defined as the active cutting points. If d_a is chosen such that β_a is equal to the angular spacing, $\beta_p = \frac{2\pi}{N}$, all cutting points on the positive β axis, and only one point at each β, will be engaged in the cutting. Such a d_a, designated as d_a^*, and the ratio

of d_a to d_a^*, defined as η_a, are expressed in

$$d_a^* = \frac{\beta_p R}{\tan\alpha}$$

and

$$\eta_a = \frac{d_a \tan\alpha}{\beta_p R} \text{ or } \eta_a = \frac{\beta_a}{\beta_p}.$$

If η_a >1, there will be an overlap of β_a-β_p in the angular cutting region between neighboring flutes, and within that region, there will be more than one active cutting points at each β, which are located on different flutes and separated by d_a^* in the axial position. Alternatively, using h as an independent variable, Equation 3 can be rewritten as

$$\beta_k(h) = \frac{\tan\alpha}{R} + (k-1)\beta_p, \qquad k = 1, 2 \ldots \infty, \qquad 0 \le h \le d_a \tag{5}$$
$$r_k = R.$$

As before, this expression is only defined for values of h within the axial depth of cut. As a result the axial position for any cutting point can be found using Equation 3 given its flute number k and angular position β. The angular position of that point can also be found using Equation 5 given it's axial position and flute number. This βrh coordinate system will be referred to as the cutter coordinate system from now on.

A second, non-rotating rectangular coordinate system, XYZ, is attached to the bottom center of the cutter with its origin coinciding with the origin of the βrh frame. For the following calculations it is assumed that the cutter moves in the X direction at the speed of t_x per tooth although in actual cutting the cutter is stationary and the workpiece moves in the negative X direction. Also, an angular position variable θ in the XYZ coordinate system is defined to represent the angular position of the cutting point in the workpiece as shown in Figure 6. This XYZ coordinate system is called the work coordinate. The cutter rotates about the Z axis with an angular velocity Ω, and the angular displacement of the cutter with respect to the XYZ frame is represented by ϕ=Ωt. The angular position θ in the work of any cutting point at position β on the cutter is therefore

$$\theta(\phi, \beta) = \phi - \beta. \tag{6}$$

2.4 Chip Thickness

The conventional cutting force model[31][37] is based on three assumptions: (1)$F_t = K_t b t_c$, the tangential cutting force is proportional to the cutting area, (2) $F_r = K_r F_t$, the radial cutting force is proportional to the tangential cutting force, and (3)$t_c = t_x \sin\theta$, the chip thickness is a function of feed and the angle of the cutting point. This simplification is made by assuming that the trajectory of the tool is circular. However, since higher feeds are used in MEMO, the first two assumptions hold but the third assumption fails. The true trochoidial path must be taken into consideration. The true chip thickness is developed in the following sections.

2.4.1 CEMO Chip Thickness

The general chip thickness equation for an active cutting point on a cutter in a CEMO without runout can be approximated as [25]

$$t_{c,CEMO}(\theta) = t_x sin\theta. \tag{7}$$

In this expression, the tooth trajectory of a milling cutter was assumed to be circular, as shown in Figure 2, instead of trochoidial. Therefore the equation is not an exact solution for the chip thickness. However it is a good approximation when feed per tooth is much less than the cutter diameter, a condition that is true in CEMO. Equation 7 has been widely used for the analysis of the milling process. The cutter entry and exit angles θ_{1r} and θ_{2r}, and radial range of cutting, θ_{rr}, are dictated by the radial depth of cut, d_r, and cutter recess ,c, as shown in Figure 6 and are expressed by

$$\begin{aligned} \theta_{1r} &= \cos^{-1}(1 - 2\eta_c) \\ \theta_{2r} &= \cos^{-1}(1 - 2(\eta_r + \eta_c)) \\ \theta_{rr} &= \theta_{2r} - \theta_{1r} \end{aligned} \tag{8}$$

where

$$\eta_r = \tfrac{d_r}{D} \text{ and } \eta_c = \tfrac{c}{D}.$$

Some geometrical approximations are made in Equation 8 especially around the extreme values of 0 and 180 degrees. From Equation 8, the minimum entry and maximum exit angle is slightly less than 0 and the exit angle is slightly larger tnan 180 degrees. By defining a rectangular radial cutting window function,

$$w(\theta) = \begin{cases} 1, & \theta_{1r} \leq \theta \leq \theta_{2r} \\ 0, & otherwise \end{cases} \tag{9}$$

the chip thickness equation can be rewritten to reflect the radial cutting configuration and Equation 7 becomes

$$t_c(\theta, \beta) = t_x \sin\theta w(\theta). \tag{10}$$

This chip thickness equation for an end mill with no runout has dependance upon t_x and θ and is true for any active cutting point on the end mill.

If $w(\theta)$ is a value between 0 and $\frac{\pi}{2}$, it is considered to be in the up-cut or conventional milling configuration, where the cutting points move in the opposite direction of the feed of the workpiece. On the other hand, if $w(\theta)$ lies within $\frac{\pi}{2}$ and π, the cutting configuration is referred to as down-cut or climb milling, where the cutting points move in the same direction as the workpiece. Symmetric cutting has properties of both cutting configurations because the center of $w(\theta)$ is at $\theta = \frac{\pi}{2}$. As a result the first half of the radial cutting range is classified as being in the up-cut and the second half is classified as being in the down-cut range. When $\eta_r = 1$, cutting is in the full-cut or slotting configuration with the radial cutting range spanning from 0 to π. Although the workpiece recess, c, is not required to be zero for an up-cut milling operation, it is assumed in this work that c is zero, or entry angle θ_{1r} is zero, for up-cut as is the case in common practice. Similarly, in the down-cut configuration, it is assumed that $c = D - d_r$, or the exit angle θ_{2r} is π.

2.4.2 MEMO Chip Thickness

The previous subsection defined the chip thickness in CEMO. This definition was based on the assumption that the trajectory of the cutter was circular as in Figure 2 rather than the more accurate trochoidial path of Figure 3. In the typical MEMO, with a large feed per tooth to tool radius ratio, (τ_r), the trochoidial path can not be neglected.

Bao and Tansel [3] derived expressions for chip thickness in MEMO based on the true trochoidial trajectory. Their derivation is used in this work and it is shown in the following. In end-milling operations the trajectory of the tool tip can be written as

$$x = \frac{ft}{60} + R\sin\left(\omega t - \frac{2\pi z}{N}\right) \tag{11}$$

$$y = R\cos\left(\omega t - \frac{2\pi z}{N}\right) \tag{12}$$

and the trajectory of tool cutting edges can be written as

$$\left(x - \frac{ft}{60}\right)\cos\left(\omega t - \frac{2\pi z}{N}\right) - y\sin\left(\omega t - \frac{2\pi z}{N}\right) = 0 \tag{13}$$

where $\omega = \frac{2\pi n}{60}$, N = 2 and z = 0, 1 for two-flute tools, and N = 4 and z = 0 , 1, 2, 3 for four-flute tools.

The intersection of the first cutting edge tip at time t_0 with angle θ_0 and the second cutting edge time t_1 with angle θ_1 is solved from Equations 11,12, and 13:

$$\frac{f}{60\omega}(\omega t_0 - \omega t_1)\cos\left(\omega t_1 - \frac{2\pi(z+1)}{N}\right) + R\sin\left(\omega t_0 - \omega t_1 + \frac{2\pi}{N}\right) = 0.$$

Next, geometric conditions are considered in order to show that

$$\frac{f}{2\pi n}\left(\frac{2\pi}{N} - \delta\right)\cos\left(\frac{\pi}{2} - \theta_1\right) = R\sin\delta$$

where

$$\theta_z = \left(1 + \frac{4z}{N}\right)\frac{\pi}{2} - \omega t_z \tag{14}$$

$$\delta = \theta_{z+1} - \theta_z \tag{15}$$

$$\omega t_{z+1} - \omega t_z = \frac{2\pi}{N} - \delta. \tag{16}$$

From the above equation, the computing angle δ can be solved and is given by

$$\delta \approx \frac{t_x \frac{\cos\theta}{R}}{1 + t_x \frac{N\cos\theta}{2\pi R}}$$

where

$$t_x = \frac{f}{nN} \tag{17}$$

$$\theta = \frac{\pi}{2} - \theta_1. \tag{18}$$

The computing feed rate is defined as

$$f_c = \frac{f}{60}(t_1 - t_0),$$

or considering geometric conditions and substituting in δ, it can be rewritten as

$$f_c = \frac{f}{2\pi n}\left(\frac{2\pi}{N} - \delta\right) \approx t_x\left(1 - t_x\frac{N\cos\theta}{2\pi R}\right).$$

Next it is shown that from the geometry, R^2 can be represented as

$$R^2 = H^2 + f_c^2 - 2Hf_c\cos(\pi - \theta_1).$$

The non-cutting edge length H can be solved from the above equation and is

$$H = -f_c\sin\theta + \sqrt{R^2 - (f_c\cos\theta)^2}.$$

The resulting chip thickness is

$$t_{c,MEMO} = R - H = R + f_c\sin\theta - \sqrt{R^2 - (f_c\cos\theta)^2}.$$

Substituting the computing feed rate f_c into the above expression and simplifying it, the chip thickness expression is

$$t_{c,MEMO} \approx t_x\sin\theta - \frac{N}{2\pi R}t_x^2\sin\theta\cos\theta + \frac{1}{2R}t_x^2\cos^2\theta. \tag{19}$$

Note that this is the corrected form of $t_{c,MEMO}$ that was initially presented by Bao et al.[3].

If the physical meaning of each term of the expression in Equation 19 is evaluated, the first term is a major contributor to the chip thickness. In the conventional model, only this term was considered. The second term presents the difference between up and down-milling. It is a negative value when θ is changed from 0 to $\frac{\pi}{2}$ radians and a positive value from $\frac{\pi}{2}$ to π radians. In other words, the chip thickness of down-milling is always bigger than up-milling. The third term is an additional chip thickness. In Tlusty and Macneil's model, chip thickness is equal to zero when $\theta = n\pi$ radians, where $n = 0, 1, 2, \cdots\infty$. However, according to Equation 19, the chip thickness is not equal to zero.

2.5 Average Chip Thickness

The average chip thickness in the presence of cutter runout in CEMO has been successfully used in the prediction of cutting forces [17]. It is defined as the total chip volume removed in one revolution divided by the total area of actual cutting region in the β-θ plane and can be expressed as

$$\begin{aligned} \bar{t}_{c,CEMO} &= \frac{\sum_{k=1}^{N} \int_{(k-1)\frac{2\pi}{N}}^{(k-1)\frac{2\pi}{N}+\beta_a} \int_{\theta_{1r}}^{\theta_{2r}} t_x \sin\theta d\theta d\beta}{\sum_{k=1}^{N} \int_{(k-1)\frac{2\pi}{N}}^{(k-1)\frac{2\pi}{N}+\beta_a} \theta_2(\beta) - \theta_1(\beta) d\beta} \\ &= \frac{2N\beta_a t_x \eta_r}{\sum_{k=1}^{N} \int_{(k-1)\frac{2\pi}{N}}^{(k-1)\frac{2\pi}{N}+\beta_a} \theta_2(\beta) - \theta_1(\beta) d\beta}. \end{aligned} \tag{20}$$

Considering Equation 19 for chip thickness in MEMO the expression for average chip thickness becomes

$$\begin{aligned} \bar{t}_{c,MEMO} &= \frac{\sum_{k=1}^{N} \int_{(k-1)\frac{2\pi}{N}}^{(k-1)\frac{2\pi}{N}+\beta_a} \int_{\theta_{1r}}^{\theta_{2r}} t_x \sin\theta - \frac{N}{2\pi R} t_x^2 \sin\theta\cos\theta + \frac{1}{2R} t_x^2 \cos^2\theta d\theta d\beta}{\sum_{k=1}^{N} \int_{(k-1)\frac{2\pi}{N}}^{(k-1)\frac{2\pi}{N}+\beta_a} \theta_2(\beta) - \theta_1(\beta) d\beta} \\ &= \frac{2N\beta_a t_x \eta_r + \frac{N^2\beta_a}{8\pi R} t_x^2 (\cos 2\theta_{2r} - \cos 2\theta_{1r}) + \frac{N\beta_a}{8R} t_x^2 (2\theta_{rr} + \sin 2\theta_{2r} - \sin 2\theta_{1r})}{\sum_{k=1}^{N} \int_{(k-1)\frac{2\pi}{N}}^{(k-1)\frac{2\pi}{N}+\beta_a} \theta_2(\beta) - \theta_1(\beta) d\beta}. \end{aligned} \tag{21}$$

If runout does not exist, the denominator in the expressions for average chip thickness is simply $N\beta_a\theta_{rr}$ and Equations 20 and 21 are reduced to the expression for the average chip thickness of a true cutter in CEMO and MEMO,

$$\bar{t}_{c,CEMO} = \frac{2t_x\eta_r}{\theta_{rr}} \tag{22}$$

$$\begin{aligned} \bar{t}_{c,MEMO} &= \frac{2t_x\eta_r}{\theta_{rr}} + \frac{Nt_x^2}{\theta_{rr} 8\pi R}(\cos 2\theta_{2r} - \cos 2\theta_{1r}) \\ &\quad + \frac{t_x^2}{8R\theta_{rr}}(2\theta_{rr} + \sin 2\theta_{2r} - \sin 2\theta_{1r}). \end{aligned} \tag{23}$$

2.6 Summary

In this chapter conventional end milling and micro end milling operations were shown to be fundamentally different, based upon a higher feed per tooth per tool radius ratio used. After these two operations were defined, the derivations of chip thickness in both operations were presented. Subsequently, expressions for average chip thickness in CEMO and MEMO were given and will be used in the determination of radial and tangential forces.

CHAPTER III

EMPERICAL CUTTING COEFFICIENTS IN MEMO

3.1 Introduction

The milling force model is an important part in understanding the the physics of the cutting process. In the following sections, cutting force models are introduced. Also, the recent research in cutting pressure constants is introduced.

3.1.1 Modeling Cutting Forces

Milling is a versatile process at conventional sizes and at the micro-scale. A drawback is the slow material removal rates that limit productivity and add cost to the machined parts. However, for prototyping and the fabrication of replication masters, particularly for microfluidic applications, micro milling can economically compete with other processes. Micro-scale cutting forces must be reduced to acceptable levels that will ensure long tool life yet reasonable removal rates. The ability to quickly predict the machining forces dominated by parasitic contact friction is necessary for better process planning. Knowing the forces present during micro-milling can also help to reduce or eliminate tool breakage.

Accurate modeling of the cutting forces is required to predict the cutting forces, vibration, surface quality, and stability of machining processes. A number of different methods to predict cutting forces have been developed over the last fifty years. These models can be classified into three major categories: empirical, analytical, and mechanistic methods.

In the empirical methods, a number of machining experiments are performed and performance measures such as cutting force, tool life, and tool wear are measured. These results are then correlated to the cutting conditions using empirical functions. The empirical methods often require a lot of experimentation and have limited extrapolative value. Analytical approaches[42][30] model the physical mechanisms that occur during cutting. However due to complex mechanisms such as high strain rates, high temperature gradients and combined

elastic and plastic deformations the analytical models are unable to completely characterize the phenomena that occur on the rake and flank face of the cutting insert.

Mechanistic models[45][28] predict the cutting forces based on a method developed by Sabberwal [18]. In this method, the cutting force is assumed to be proportional to the chip cross sectional area. The constants of proportionality are called the specific cutting pressures and depend on the cutter geometry, cutting conditions, insert grade and workpiece material properties. The specific cutting pressures are typically obtained from calibration tests. Traditionally, the calibration of the cutting force model is performed by running tests at different combinations of spindle seed, feed rate and depth of cut. In face milling, these tests are conducted using a single cutting insert to avoid the effects of runout. In addition these tests are conducted on a workpiece with no surface discontinuities to simplify the correlation of the cutting forces with the angular position of cutting insert.

3.1.2 Specific Cutting Pressures

The item that is of most benefit to machine tool operators is a coefficient that will produce an estimate of the forces in the milling process based on machining parameters. This coefficient is termed the specific cutting pressure.

An empirical equation was proposed to relate the tangential cutting force to the chip thickness by a specific cutting pressure constant K_t [18], which was determined by experimental data. The above results have been followed by many authors to explore the field of the end milling force system. Budak and Altintas [8] predicted the milling force coefficients from orthogonal cutting data. Yucesan and Altintas [45] improved the cutting force coefficient's model in peripheral milling. They derive a nonlinear cutting force coefficient model, so the cutting force coefficients must use 6th order polynomials via the inverse transformation. Basically, these approaches derived complicated cutting force models and required the the knowledge of some specific parameters which cannot be easily determined.

Martellotti [25][26] indicated that the instantaneous chip thickness of the undeformed cross-section of the chip is one of the basic elements in the milling process. Koenigsberger and Sabberwal [20] assumed that the cutting force is equal to the area of the chip-section

multiplied by a specific cutting pressure. The specific cutting pressure was shown to be a function of the chip thickness for slab and face milling. Sabberwal[31] found that the specific cutting pressure in down-milling is higher than that in up-milling. The specific cutting pressure was calculated by dividing the tangential force at an instant by the corresponding chip section. Zhou and Wang[46] showed that the tangential cutting force is equal to the area of the chip-section multiplied by specific tangential cutting pressure constant, and the radial force is equal to the tangential cutting force multiplied by a cutting force ratio. Both specific tangential cutting force and the cutting force ratio were determined by experimental data using fly cutting.

Recently, Tansel et al. [34][35][36] explored the wear and failure mechanisms of micro end mills while machining aluminum graphite, and steel workpieces. The two techniques they used were acoustic emission signals and monitoring of cutting force variation. After developing a model to predict the failure of micro end mills, they focused on extending tool life with a smart workpiece holder. Bao and Tansel[3][4][5] studied the micro-milling process using 700 micron diameter high speed steel and carbide milling tools on aluminum, steel, and copper. The model was based on the assumption that the tangential cutting force is proportional to the uncut chip area and the radial cutting force is proportional to the tangential cutting force and on the trochoidial nature of the tool path. This body of knowledge has aided in the understanding of forces in micro end milling. However, the need to understand cutting coefficients in the micro end milling operation still exists.

Section 3.2 describes the design process and selection of components for a micro machining center developed at Georgia Tech. The experimental procedure for obtaining forces in the micro end milling operations is presented in Section 3.3. The decomposition of those forces into the desired cutting pressures is outlined in section 3.4. Finally, the new model for cutting coefficients in micro end milling operations is presented in section 3.5.

3.2 Aparatus

A micro machining center was designed and built by researchers in Georgia Tech's Precision Machining Research Consortium (PMRC) in order to research and understand machining

processes on the micro and meso scales. This research was conducted in conjunction with the engineers of PMC Inc. in Taiwan.

There were several requirements in the design of the micro machining center. In micro-machining engineers can either manufacture complete micro-scale parts or they can focus on creating micro-features on larger parts. Therefore the working volume of the machine can be relatively small. Miniaturization of the tool also has the benefit of increasing the dynamic and static stiffness compared to larger machine tools. There are similar improvements in thermal response, reduction of power consumption, and reduction of workpiece costs and waste. Because of these anticipated benefits, the PMRC designed and built a machine tool that would be a fraction of the size of standard machine tools but maintain the same level of quality in the finished product. Therefore the micro machining center was required to be small in size, extremely precise, and resist errors caused by thermal and dynamic interferences. A great deal of time was spent selecting components that would meet these requirements. These components are explained in more detail in the following paragraphs.

The frame serves as the backbone of the machine tool and was one of the first components to be designed. When designing the machine tool frame the PMRC considered what form factor the frame should take and what material the frame should be made out of. Common form factors for machining centers include the Bridgeport, the gantry, and the hexapod.

The gantry form factor usually consists of 2 columns which support a vertical spindle over the workpiece. One of the benefits of the gantry form factor is that it has a closed force loop, which provides a greater resistance against deflection than similarly sized Bridgeport frames. The down side is that the extra columns increase the overall size of the machine tool and also hinder access to the workpiece.

The hexapod form factor is an arrangement of six variable length struts that replace the sliding beams and rotating members of conventional orthogonal machines[15]. This technology provides the possibility to make machines that compete with human adaptability and dexterity. Hexapods are are scaleable in size, both upwards and downwards, to accommodate a multitude of applications. Hexapods are inherently rigid due to their design geometry. The mechanisms make effective use of triangles, being the strongest geometric

structure, i.e., a geodesic dome. Hexapods are also modular and do not need a foundation. Thus a hexapod could potentially function laid on its side or suspended from the ceiling. On the other hand, hexapods require large external hydraulic units to power the struts, they can be costly, and the control algorithms for hexapods are still being researched.

As the name implies, the Bridgeport form factor is that of single column vertical milling machines which were made popular in the 1930's by the Bridgeport Machines Co. of Bridgeport, Connecticut[1]. This form factor is uncomplicated, it is less expensive than a gantry or hexapod of similar size, allows ease of access to the workpiece, and takes up less space than gantry or hexapod based frames of similar size. For these reasons the frame of the micro machining center was designed with the Bridgeport form factor.

Once the form factor was selected for the machine tool frame, the next item considered was what material the frame should be made of. Carpenter Invar 36 was the material of choice because it met all of our requirements: it has a hardness and strength that is comparable with other common structural materials, and yet it has an extremely low coefficient of thermal expansion. The effects of machining loads and thermal gradients on the quality of the machined components would be minimized as a result of building the frame with Invar.

Another component considered was the positioning system for the micro machining center. Two technologies used for precision positioning include electronic linear motors and piezoelectric drives. Both of these technologies have been shown to have positioning accuracies on the sub-micron level. The piezoelectric effect is an on-off phenomenon which occurs in materials which couple dielectric polarization and strain, which results in a deflection under an applied voltage. The induced strain is small which results in a highly accurate yet relatively small range of motion. Linear motors, on the other hand, often have higher minimum resolutions than piezoelectric drives but larger ranges of travel. Although linear motors are typically larger than piezoelectric drives they do allow for variable drive speeds. The micro machining center developed by the PMRC uses an AeroTech linear positioning system. Linear brush-less DC motors provide motion for the 3 axes which have a minimum achievable resolution of 2nm.

Additional considerations were made in the selection of a spindle and vision system for the micro machining center. The spindle must have a low runout and a high stiffness as errors in these two errors are magnified with miniaturization. Also the spindle must be capable of generating extremely large spindle speeds in order to produce high material removal rates. Vision systems are important because as the tool size decreases, tactile feedback is almost eliminated. The vision system facilitates the setup of the machining process and in the monitoring of the cutting process.

The previous considerations were taken into account when designing a machine tool for micro milling operations. The next section describes how this newly developed micro machining center was used to experimentally determine cutting coefficients in MEMO.

3.3 Experiment

A figure of the typical experimental setup is shown in Figure 4. The micro-machining center developed by the PMRC was used to conduct the experiments. The 7075-T6 Aluminum workpiece was fixtured to the Kistler Dynamometer which was mounted to the Aerotech positioning stage. Two components of the cutting forces were transfered by a charge amplifier and recorded using a National Instruments DAQ card and LabView program.

The purpose of this experiment was to increase chip thickness and measure the corresponding tangential and radial cutting forces. The machining process has several user-defined parameters including axial depth of cut, radial depth of cut, spindle speed, and feed. Average chip thickness is proportional to t_x and η_r, and inversely proportional to θ_{rr} as shown in Equation 23. Thus increasing t_x, increasing η_r or decreasing θ_{rr} will all produce a corresponding increase in t_c. In this experiment d_r, and thus η_r, was increased while all other cutting parameters were held constant. The milling process was down-milling and the radial depth of cut varied from $d_r = 10$ microns to a full cut condition of $d_r = 800$ microns. Average forces F_x and F_y, parallel and perpendicular to the feed motion, respectively, were recorded over a travel of five mm.

3.4 Analysis

The coordinate system of the model is presented in Figure 6. For a certain tool cutting angle, θ, the chip thickness t_c is not constant but a function of h because of the tool helix angle, α.

$$dF_t = K_t t_c(h) dh$$

where

$$h = h(\theta)$$
$$dh = \frac{R}{\tan\alpha} d\theta.$$

Tangential and radial forces depend upon t_c in the following way:

$$F_t = K_t b t_c \tag{24}$$

$$F_r = K_t K_r F_t \tag{25}$$

and can be rewritten as

$$dF_t = \frac{K_t R}{\tan\alpha} t_c(\theta) d\theta \tag{26}$$
$$dF_r = \frac{K_t R}{\tan\alpha} K_r t_c(\theta) d\theta. \tag{27}$$

The cutting forces in feed and normal directions can be expressed as

$$dF_x = dF_t \cos\theta + dF_r \sin\theta = \frac{K_t R}{\tan\alpha} t_c(\theta)(\cos\theta d\theta + K_r \sin\theta d\theta) \tag{28}$$
$$dF_y = dF_t \sin\theta - dF_r \cos\theta = \frac{K_t R}{\tan\alpha} t_c(\theta)(\sin\theta d\theta - K_r \cos\theta d\theta). \tag{29}$$

Substituting in the equations for $t_{c,MEMO}$ yields

$$dF_x = \frac{K_t R t_x}{\tan\alpha}\left(\sin\theta - \frac{N}{2\pi R} t_x \sin\theta\cos\theta + \frac{1}{2R} t_x \cos^2\theta\right)(\cos\theta d\theta + K_r \sin\theta d\theta) \tag{30}$$
$$dF_y = \frac{K_t R t_x}{\tan\alpha}\left(\sin\theta - \frac{N}{2\pi R} t_x \sin\theta\cos\theta + \frac{1}{2R} t_x \cos^2\theta\right)(\sin\theta d\theta - K_r \cos\theta d\theta). \tag{31}$$

Taking integration, the cutting force expressions become

$$F_x = \frac{K_t R t_x}{2\tan\alpha}\Big[\frac{1}{3}\left(1+K_r\frac{N}{\pi}\right)\frac{t_x}{R}\sin^3\theta + \frac{1}{3}\left(K_r-\frac{N}{\pi}\right)\frac{t_x}{R}\cos^3\theta - \sin^2\theta + \frac{1}{2}K_r\sin(2\theta) - \frac{t_x}{r}\sin\theta - K_r\theta\Big]\Big|_{\theta_{1r}}^{\theta_{2r}} \tag{32}$$

$$F_y = \frac{K_t R t_x}{2\tan\alpha}\Big[\frac{1}{3}\left(K_r-\frac{N}{\pi}\right)\frac{t_x}{R}\sin^3\theta - \frac{1}{3}\left(1+K_r\frac{N}{\pi}\right)\frac{t_x}{R}\cos^3\theta - K_r\sin^2\theta - \frac{1}{2}\sin(2\theta) - K_r\frac{t_x}{r}\sin\theta + \theta\Big]\Big|_{\theta_{1r}}^{\theta_{2r}}. \tag{33}$$

This can be solved by rewriting the above in matrix form

$$\begin{pmatrix} F_x \\ F_y \end{pmatrix} = \frac{t_x R}{2\tan\alpha}\begin{bmatrix} P_1 & P_2 \\ P_2 & -P_1 \end{bmatrix}\begin{pmatrix} K_t \\ K_t K_r \end{pmatrix} \tag{34}$$

where

$$P_1 = \left[\sin^2\theta + \frac{N}{\pi R}t_x\frac{\cos^3\theta}{3} + \frac{t_x}{R}\left(\sin\theta - \frac{\sin^3\theta}{3}\right)\right]\Big|_{\theta_{1r}}^{\theta_{2r}} \tag{35}$$

$$P_2 = \left[\theta - \frac{\sin 2\theta}{2} - \frac{N}{\pi R}\frac{\sin^3\theta}{3} - \frac{t_x}{R}\frac{\cos^3\theta}{3}\right]\Big|_{\theta_{1r}}^{\theta_{2r}}. \tag{36}$$

Solving for K_t and K_r yields

$$\begin{aligned}\begin{pmatrix} K_t \\ K_t K_r \end{pmatrix} &= \left(\frac{t_x R}{2\tan\alpha}\right)^{-1}\begin{bmatrix} P_1 & P_2 \\ P_2 & -P_1 \end{bmatrix}^{-1}\begin{pmatrix} F_x \\ F_y \end{pmatrix} \\ &= \left(\frac{2\tan\alpha}{R t_x}\frac{1}{P_1^2+P_2^2}\right)\begin{bmatrix} P_1 & P_2 \\ P_2 & -P_1 \end{bmatrix}\begin{pmatrix} F_x \\ F_y \end{pmatrix}.\end{aligned} \tag{37}$$

This result is similar to the determination of cutting pressure constants as derived by Wang[41] and will be used to produce cutting constants based on measured forces. In his derivation a convolution model of the milling force system was created by taking the Fourier transforms of the chip width density function, tooth sequence function, and elementary cutting force functions. This yielded an expression for K_t and K_r in the frequency domain.

3.5 Results and Discussion

The constant machining parameters, measured average forces, and resulting cutting pressure constants are tabulated in Tables 1 and 2. The tool was a 2 flute solid carbide end mill

with a diameter of 800 microns. The cutting parameters d_a, f, α, β_p, β_a, d_r, and n were held constant while d_r was increased from 10 to 800 microns. The chip thickness increased as a result of increasing d_r. Also note that the feed per tooth per radius ratio, τ_r, for each test is 0.101 which is above the minimum required value for a MEMO. The milling process started as down-milling and ended as a full slot milling operation.

The measured average forces, F_x and F_y were plotted against t_c and are shown in Figures 7 and 8 respectively. These figures indicate the expected behavior that as the chip thicknesses increase so will the resultant forces experienced by the end mill. This is a good thing, but remember that F_t and F_r are the forces that will determine the specific cutting pressures, not F_x and F_y.

The values of utmost importance for predicting forces in milling operations are K_t and K_r. The equations for K_t and K_r with respect to $\bar{t}_c$ in CEMO of 7075-T6 Aluminum are known [41][17] to be

$$K_{t,CEMO} = 569.14(\bar{t}_c)^{-0.283} N/mm^2 \tag{38}$$

$$K_{r,CEMO} = 0.1468(\bar{t}_c)^{-0.364} \tag{39}$$

and the purpose of this experimentation was to determine the corresponding equations for K_t and K_r in MEMO of 7075-T6 Aluminum. Equation 37 was used to decompose the forces F_x and F_y into F_t and F_r and then to the corresponding cutting constants K_t and K_r. The results are listed in Table 2. $K_{t,MEMO}$ and $K_{r,MEMO}$ are plotted with respect to $\bar{t}_c$ in Figures 9 and 10, respectivly. A power series fit to both sets of data yields the two new empirical equations for $K_{t,MEMO}$ and $K_{r,MEMO}$:

$$K_{t,MEMO} = 0.8992(\bar{t}_c)^{-1.3089} N/mm^2 \tag{40}$$

$$K_{r,MEMO} = 51.806(\bar{t}_c)^{0.51}. \tag{41}$$

Figure 11 compares the equations for K_t in CEMO and MEMO, and Figure 12 shows the equations for K_r in CEMO and MEMO. The following observations have been made after

analyzing Figures 11 and 12: (1) $K_{r,MEMO}$ and $K_{r,CEMO}$ have the same order of magnatude and similar levels of curvature, (2) $K_{r,MEMO}$ is concave down while $K_{r,CEMO}$ is concave up, (3) $K_{t,MEMO}$ and $K_{t,CEMO}$ have the same order of magnitude and are both concave up, and (4) $K_{t,MEMO}$ has a higher level of curvature than $K_{t,CEMO}$. The fact $K_{t,MEMO}$ and $K_{t,CEMO}$ have the same order of magnitude and are both concave up is beneficial because it indicates that our experimentally determined values for K_t are reasonable. $K_{r,MEMO}$ and $K_{r,CEMO}$ have the same order of magnitude and similar levels of curvature, which again is a good thing. On the other hand, the difference in curvatures of $K_{t,MEMO}$ and $K_{r,CEMO}$, and the reason why $K_{r,MEMO}$ is concave down while $K_{r,CEMO}$ is concave up is not at first entirely obvious.

Upon further analysis of the figures and equations for K_r and K_t the reasons for the differences listed in the previous paragraph become apparent. The important thing to remember is that in MEMO extremely aggressive feeds are used compared to the radius in order to ensure that $\tau_r > 0.1$. We also see the dependance of $\bar{t}_c$ on τ_r by rewriting Equations 22 and 23 as

$$\begin{aligned}
\bar{t}_{c,CEMO} &= \frac{2t_x\eta_r}{\theta_{rr}} = \frac{2t_x\frac{d_r}{D}}{\theta_{rr}} = \frac{4d_r}{\theta_{rr}}\frac{t_x}{R} = \frac{4d_r}{\theta_{rr}}(\tau_r) \\
\bar{t}_{c,MEMO} &= \frac{2t_x\eta_r}{\theta_{rr}} + \frac{Nt_x^2}{\theta_{rr}8\pi r}(\cos 2\theta_{2r} - \cos 2\theta_{1r}) \\
&\quad + \frac{t_x^2}{8f\theta_{rr}}(2\theta_{rr} + \sin 2\theta_{2r} - \sin 2\theta_{1r}) \\
&= \frac{4d_r}{\theta_{rr}}(\tau_r) + \frac{Nt_x}{\theta_{rr}8\pi}(\tau_r)(\cos 2\theta_{2r} - \cos 2\theta_{1r}) \\
&\quad + \frac{t_x^2}{8f\theta_{rr}}(2\theta_{rr} + \sin 2\theta_{2r} - \sin 2\theta_{1r}).
\end{aligned} \tag{42}$$

This shows that t_c is proportional to τ_r and so are the forces F_t and F_r. And since the feeds used in MEMO are more aggressive than in CEMO, we expect a corresponding increase in the measured F_t and F_r.

The reasoning expressed in the previous paragraph also explains the differences in concavity and curvature. From Equations 38 and 40 for K_t we see that the power of $\bar{t}_c$ changes

from -0.283 in CEMO to -1.3089 in MEMO. Equations 39 and 41 for K_r have a change power of $\bar{t}_c$ from -0.0364 in CEMO to 0.51 in MEMO. F_t is proportional to t_c through the constant K_t and F_r is proportional to F_t through the constant K_r. K_t and K_r have been shown to have a dependance upon t_c. Since more aggressive feeds are being used it is easy to conclude that the forces seen in MEMO will be larger than those seen in a comparable CEMO. Because of the larger forces experienced in MEMO, the MEMO power regressions of Equations 40 and 41 raise $\overline{t_c}$ to powers of greater magnitude than the CEMO variants in Equations 38 and 39. Thus, the increase in magnitude of the powers in the expressions for K_t and K_r, and therefore the curvature of the functions, are dependent upon the increased forces experienced in MEMO.

In Figures 13 and 14, the tangential and radial forces were determined using the empirical cutting coefficients and are plotted with respect to average chip thickness. Both figures indicate that the forces increase as $\bar{t}_c$ increases, as expected. The two figures also show that F_t for MEMO and CEMO are of the same order of magnitude, but F_r increases as you move from CEMO to MEMO. Therefore the forces in the radial direction of the end mill will the most critical when predicting failure modes of the tool.

There are a few additional resources which support the higher forces observed in MEMO. The first is to realize that this was a down-milling operation and it has been shown by Sabberwal [31] that down-milling operations experience higher forces than in up-milling. Secondly, several studies have been conducted on single point diamond machining by Moriwak and Okuda [29] and Furukawa and Moronuki [13] using the specific cutting energy approach for diamond machining. These investigators found that as the ratio of the uncut chip thickness to the radius of the cutting edge was reduced, the specific cutting energy increased exponentially to approximately 100-times that at conventional sizes. While these experimentally determined forces do not seem to be exponentially larger there definitely is a noticeable difference in CEMO and MEMO forces.

CHAPTER IV

CONCLUSIONS

The primary contribution of this work is the analysis of micro end milling operations and the development of empirical equations to predict radial and tangential cutting coefficients in micro end milling.

Conventional end milling operations and micro end milling operations were defined as being dependent on the feed per tooth per radius ratio selected. The kinematics of the chip forming process were described and chip thicknesses for CEMO and MEMO were developed based on the tool trajectory. An expression for obtaining cutting constants from the measured forces F_x and F_y was derived. This expression was used to produce empirical equations for the cutting constants K_t and K_r.

With the completion of this thesis, the fundamentals of milling forces in micro end milling operations has been presented and the roles of various cutting parameters including axial and radial depth of cut, feed per tooth, and cutter geometry in forces on the micro scale have been explored. The tools developed in this thesis allow researchers to predict the forces experienced in a micro end milling operation and adjust cutting conditions appropriately. Based on the empirical model, further work can be completed in order to ensure maximum productivity levels in micro end milling operations.

APPENDIX A

TABLES

Table 1: Constant Cutting Conditions

d_a(mm)	0.4
D(mm)	0.8
α	30^o
β_a	$\frac{1}{\sqrt{3}}$
β_p	π
η_a	$\frac{1}{\pi\sqrt{3}}$
n(rpm)	6200
t_x(mm)	$\frac{5}{124}$
τ_r	0.101

Table 2: Cutting conditions for emperical determination of K_t and K_r. Material:7075-T6 Aluminum; Cutter geometry: N=2, D=800 microns, Helical angle: 30^o; Additional cutting parameters: Down milling operation with d_a=400 microns, β_a=0.6, $\beta_p = \pi$, Spindle speed = 6200 rpm, Feed rate = 500 $\frac{mm}{min}$, No coolant.

No.	Cutting Conditions				Meas. Avg.		Cutting Const.	
	d_r(mm)	η_c	η_r	$\bar{t}_c(10^{-3}\text{mm})$	F_x(N)	F_y(N)	$K_t \frac{N}{mm^2}$	K_r
1	0.0100	0.9875	0.0125	0.471290238	1.2565	0.8831	13296.44161	1.179871975
2	0.0200	0.9750	0.025	0.656521033	2.2158	1.7142	9834.570147	1.609708597
3	0.0300	0.9625	0.0375	0.797632165	3.8903	2.2508	11386.02538	1.411878269
4	0.0400	0.9500	0.05	0.915743383	5.2818	2.7322	10972.07328	1.44762536
5	0.0500	0.9375	0.0625	1.019051957	6.0255	2.6288	9815.201115	1.397448244
6	0.0600	0.9250	0.075	1.111769676	7.0279	2.6718	9317.995786	1.381529187
7	0.0700	0.9125	0.0875	1.196402543	7.7920	2.5682	8710.146575	1.360385195
8	0.0800	0.9000	0.1	1.274586009	8.6779	2.8838	7994.261252	1.468439197
9	0.0900	0.8875	0.1125	1.347457438	9.9080	3.7118	7317.15285	1.707140144
10	0.1000	0.8750	0.125	1.415845916	10.8194	3.8360	6966.029654	1.746843144
11	0.1100	0.8625	0.1375	1.480377917	1.1089	1.0482	130.9269938	12.8076184
12	0.1200	0.8500	0.15	1.541540497	10.7923	3.2856	5588.262056	1.762429458
13	0.1300	0.8375	0.1625	1.599721164	11.3863	3.1927	5377.511852	1.761519969
14	0.1400	0.8250	0.175	1.655234164	11.9620	3.5324	4920.009086	1.911219879
15	0.1500	0.8125	0.1875	1.70833845	5.3870	1.4578	2059.300633	1.89462342
16	0.1600	0.8000	0.2	1.759250375	13.4186	3.3936	4754.793913	1.901971285
17	0.1700	0.7875	0.2125	1.80815264	10.8630	2.4299	3657.937692	1.854693195
18	0.1800	0.7750	0.225	1.855201446	13.8206	2.0142	4787.641182	1.618324358
19	0.1900	0.7625	0.2375	1.900531191	14.1457	2.3219	4389.987973	1.746730975
20	0.2000	0.7500	0.25	1.944258567	12.1099	1.5518	3671.022574	1.667064586
21	0.2100	0.7375	0.2625	1.98648555	15.1888	0.9847	4699.436218	1.497527641
22	0.2200	0.7250	0.275	2.027301792	14.7993	2.1848	3755.993574	1.860281726
23	0.2300	0.7125	0.2875	2.066786523	15.5222	1.7162	3910.354619	1.760803301
24	0.2400	0.7000	0.3	2.105010089	15.2129	0.5226	4050.928595	1.527838705
25	0.2500	0.6875	0.3125	2.142035198	15.7688	1.2105	3699.449097	1.726642447
26	0.2600	0.6750	0.325	2.177917947	16.7042	0.2814	4067.247755	1.550609537
27	0.2700	0.6625	0.3375	2.212708669	13.2490	0.7437	2865.551417	1.738613546
28	0.2900	0.6375	0.3625	2.279190693	16.2624	0.0801	3445.105129	1.628025939
29	0.3000	0.6250	0.375	2.310959563	16.1024	2.0649	2581.494057	2.254614311
30	0.4000	0.5000	0.5	2.581295631	21.4472	0.6762	2656.568972	2.266817906
31	0.5000	0.3750	0.625	2.776266961	22.6118	5.9776	595.2545475	10.29159807
32	0.6000	0.2500	0.75	2.898269734	21.7757	9.5862	893.5466072	6.330746408
33	0.7000	0.1250	0.875	2.926513221	19.8742	8.6480	1314.606633	3.666956011
34	0.8000	0.0000	1	2.577177152	20.9580	14.1110	3202.305047	1.489589708

APPENDIX B

FIGURES

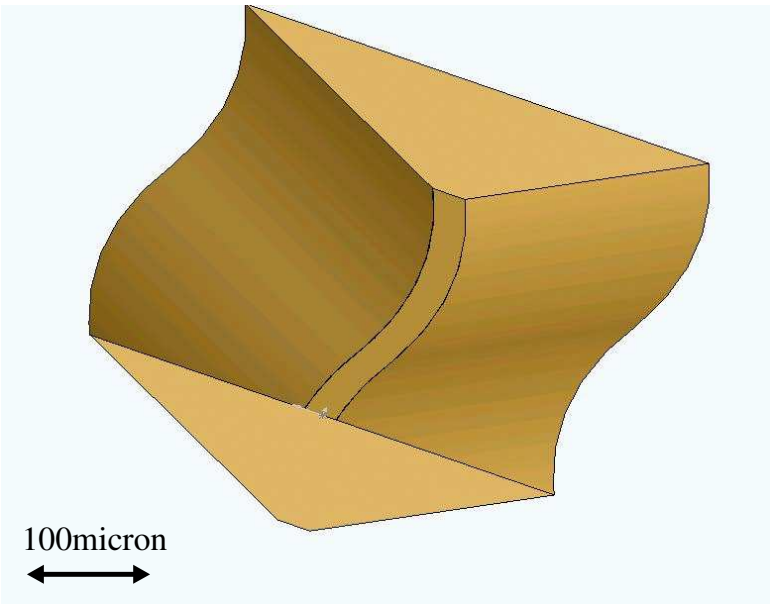

Figure 1: Sinusoidal path machined for GE Research

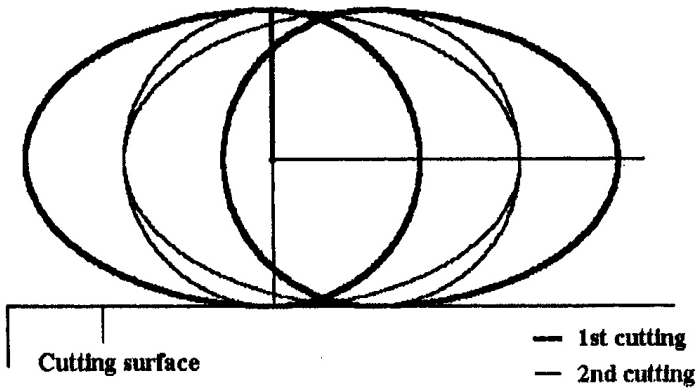

Figure 2: Conventional end milling tool path as proposed by Tlusty and Macniel [3]

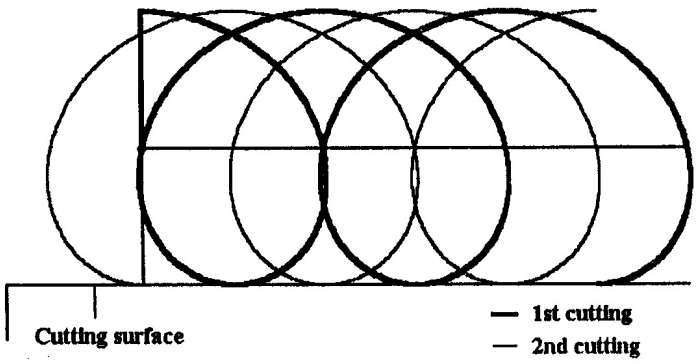

Figure 3: True trochoidial micro end milling tool path [3]

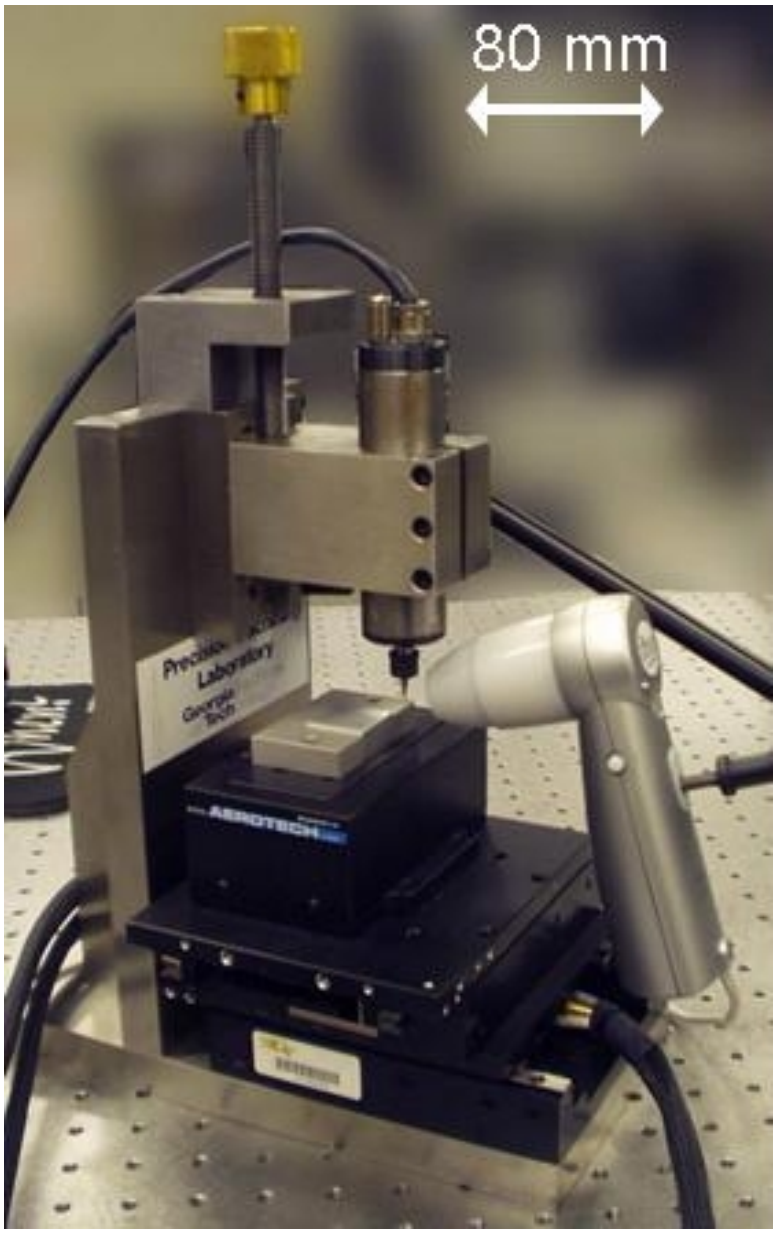

Figure 4: Micro machining center developed by PMRC

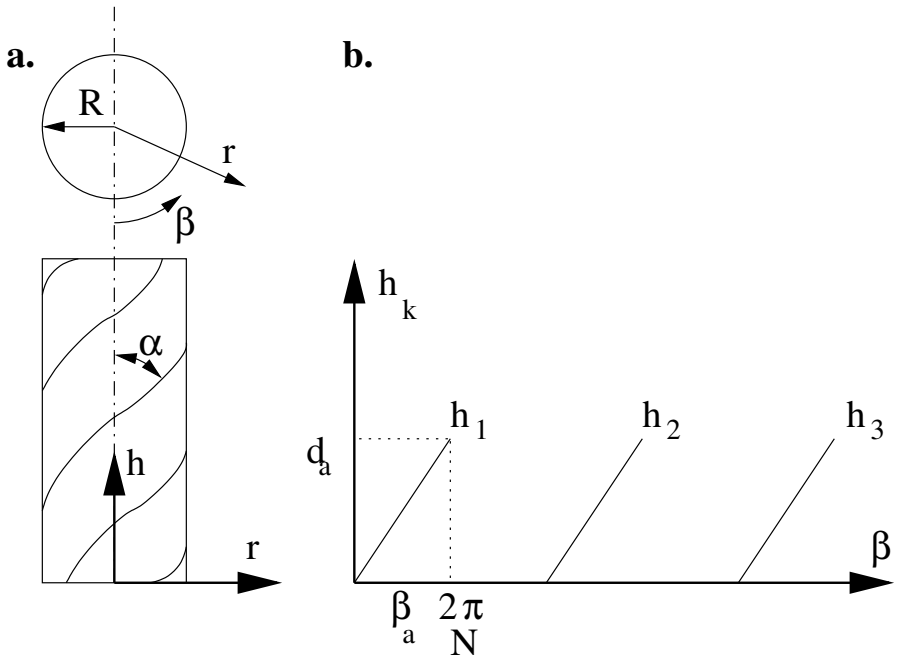

Figure 5: (a): The cylindrical cutter coordinate and (b): function h_k for cutter flute k.

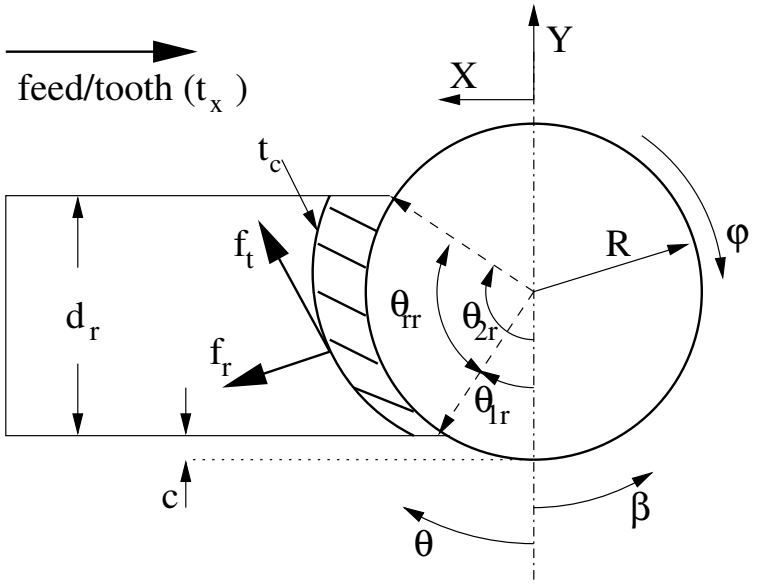

Figure 6: The radial cutting geometry in the work coordinate.

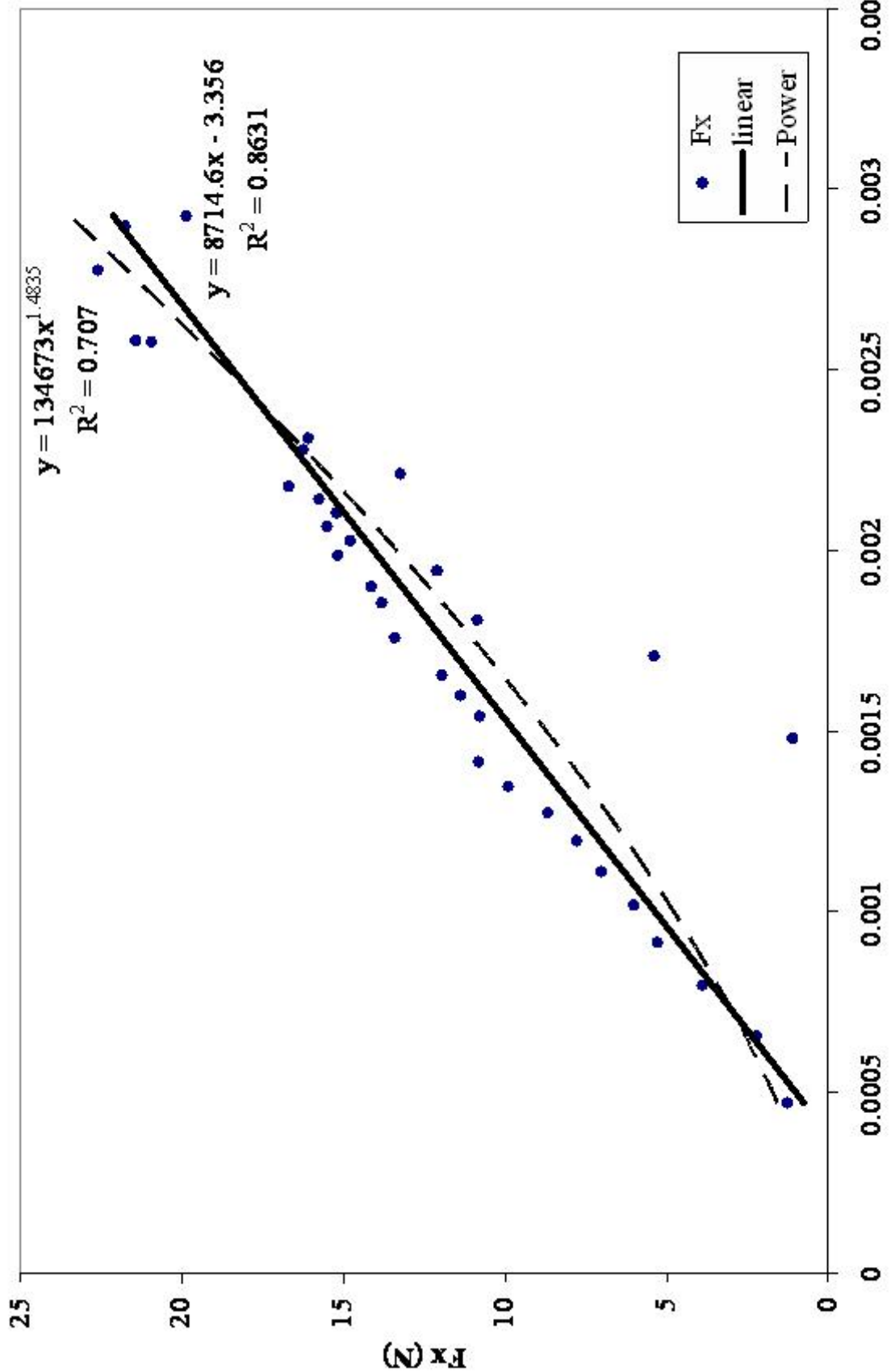

Figure 7: F_x vs. $\bar{t}_c$

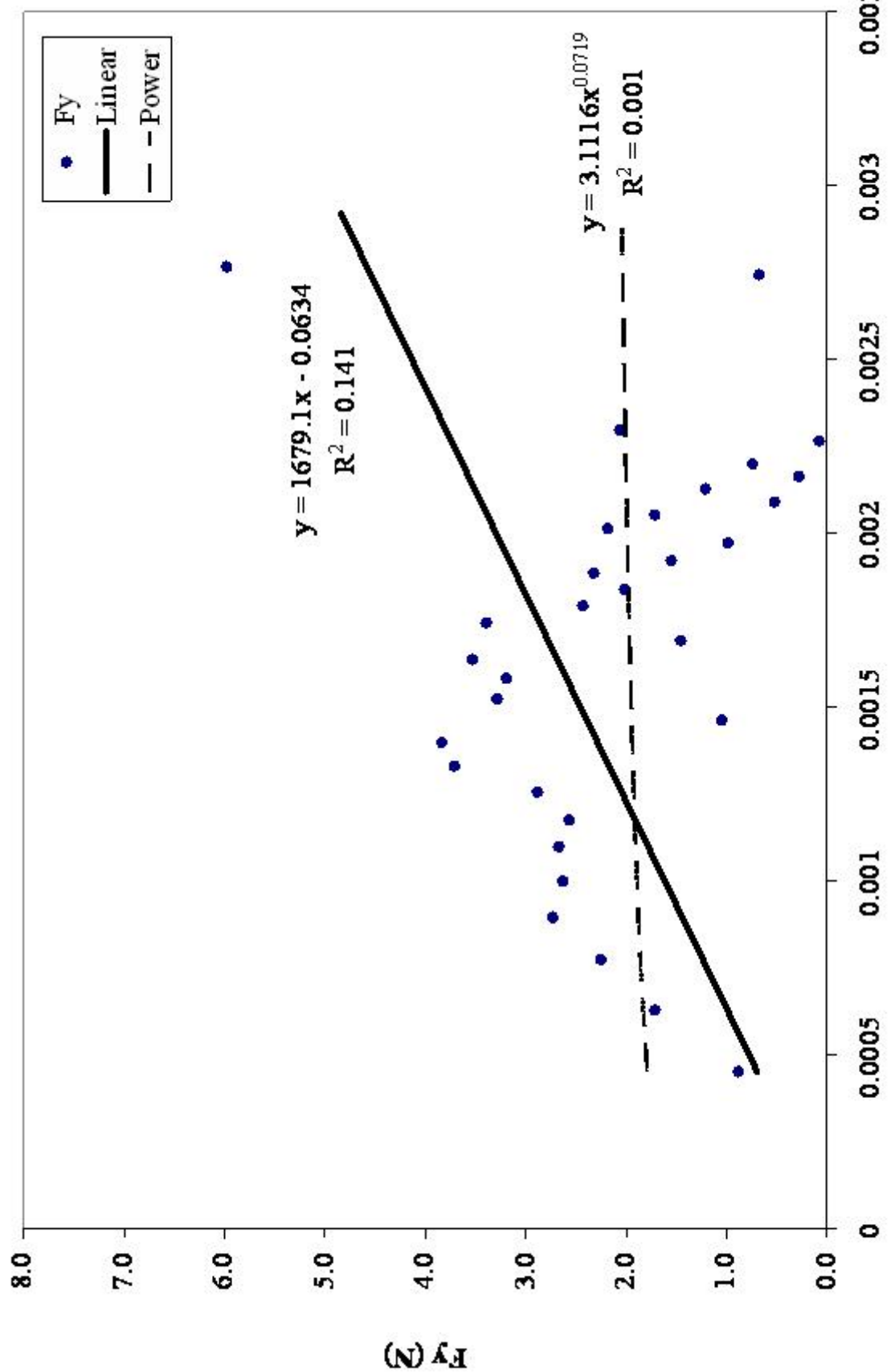

Figure 8: F_y vs. $\bar{t}_c$

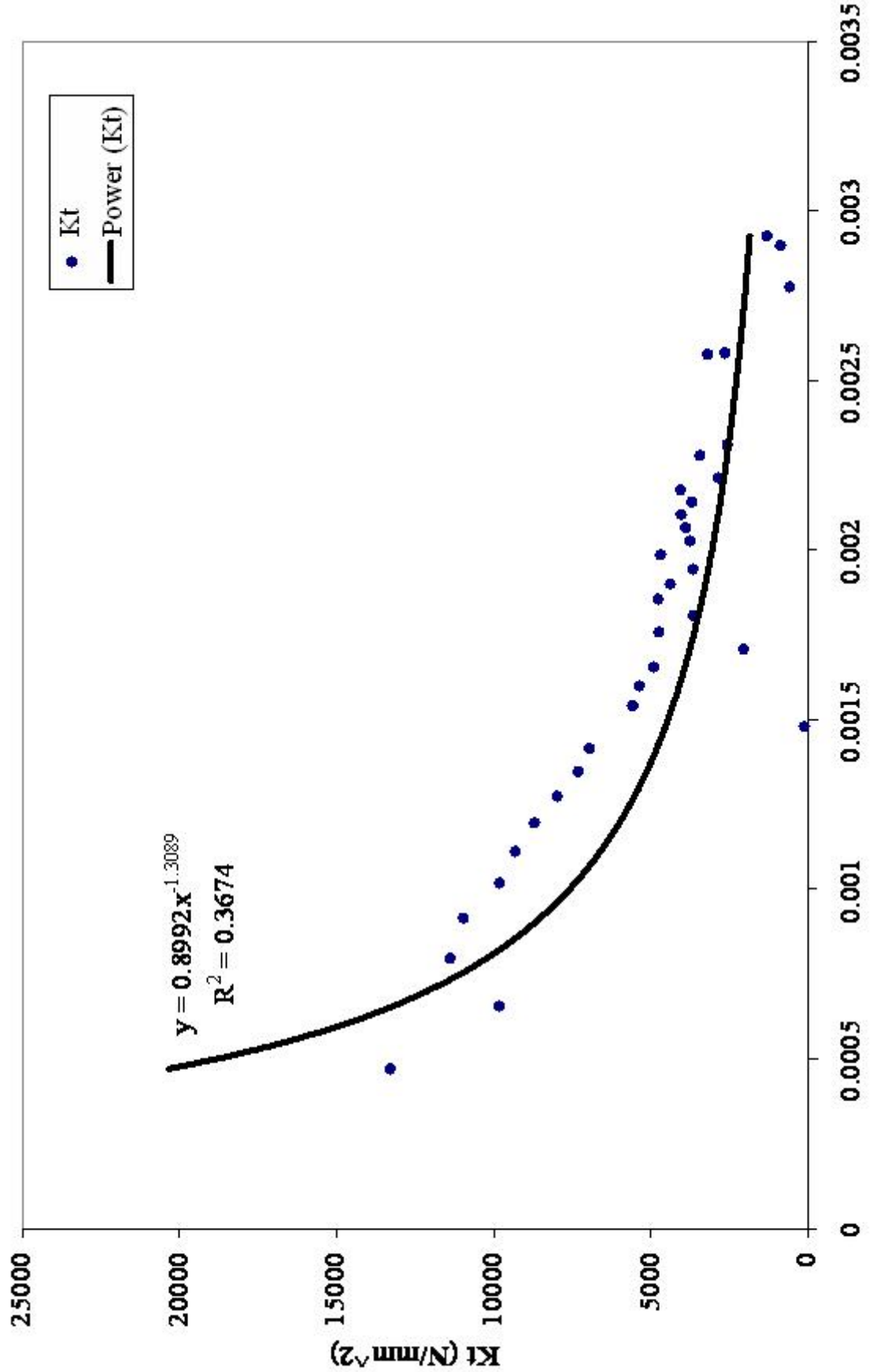

Figure 9: $K_{t,MEMO}$ vs. $\bar{t}_c$

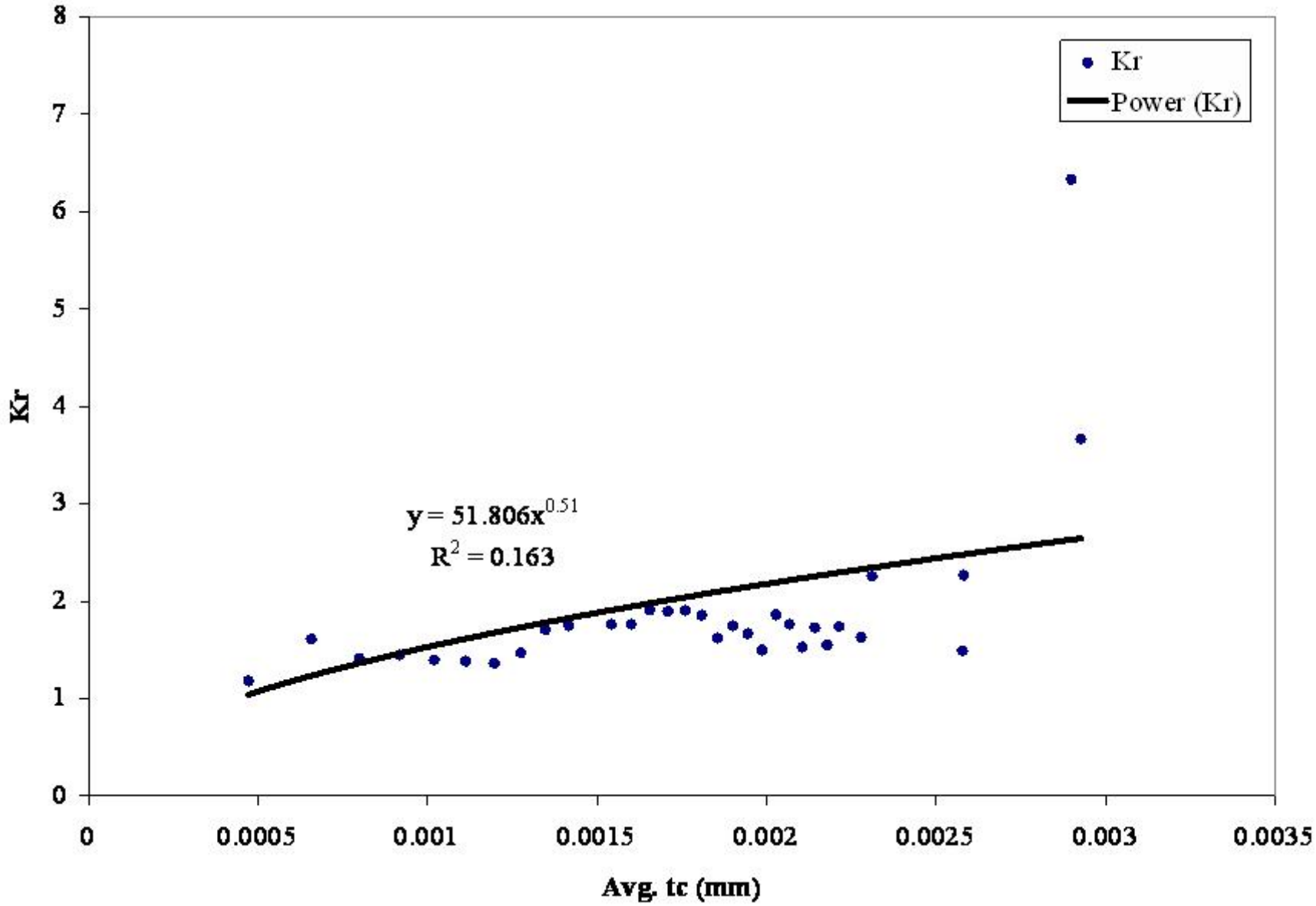

Figure 10: $K_{r,MEMO}$ vs. $\bar{t}_c$

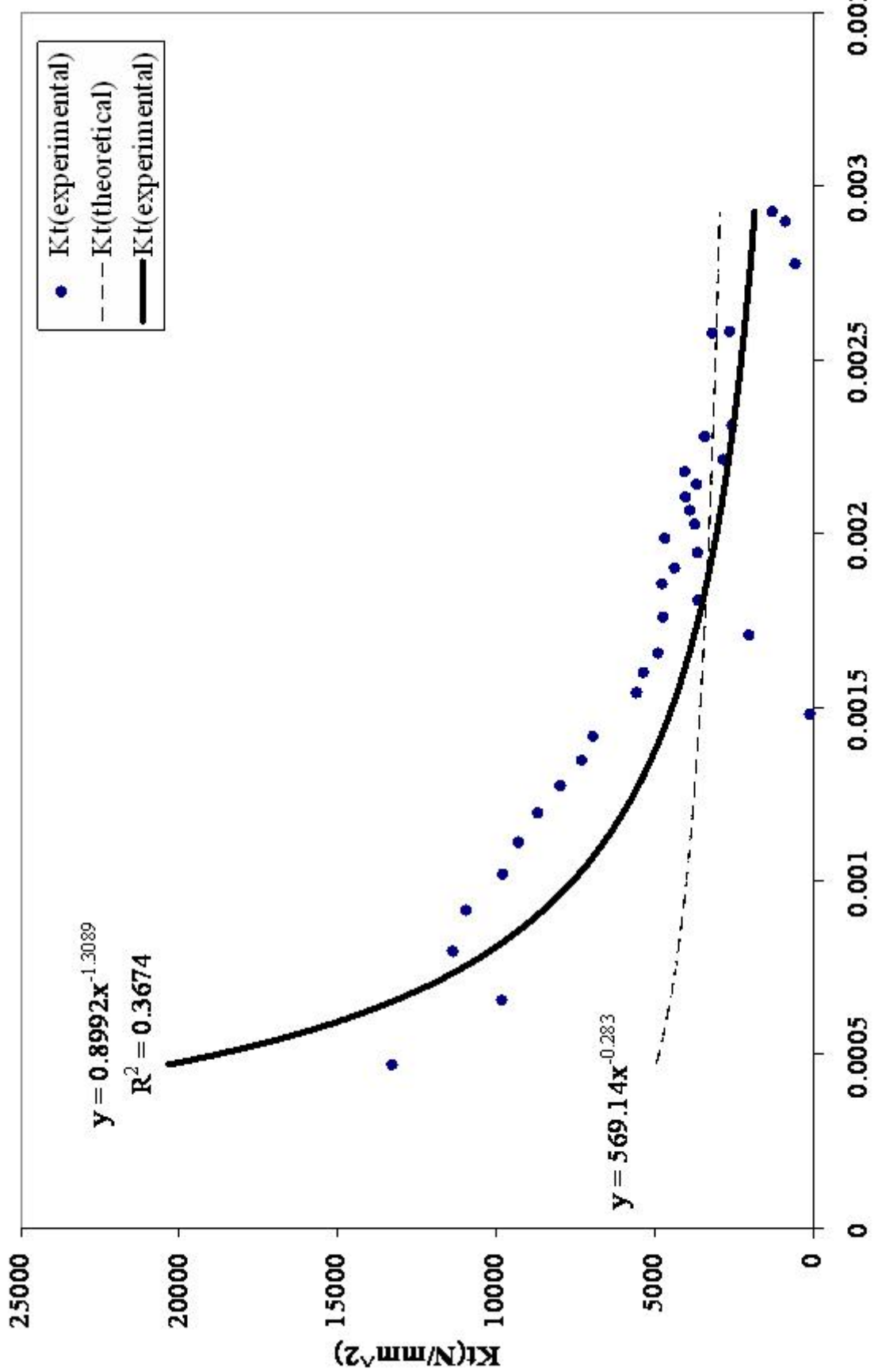

Figure 11: Comparison of $K_{t,MEMO}$ and $K_{t,CEMO}$ vs. $\bar{t}_c$

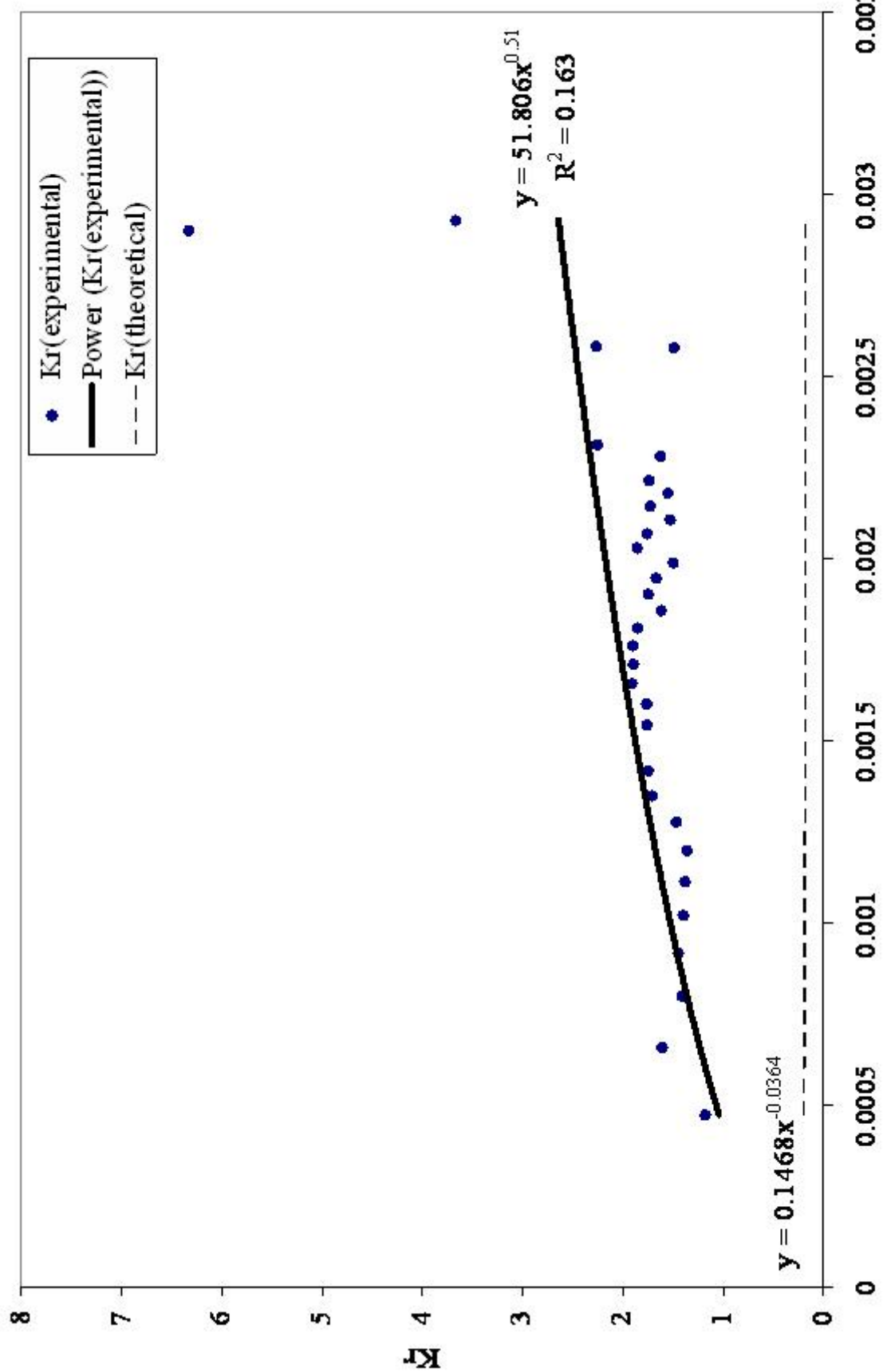

Figure 12: Comparison of $K_{r,MEMO}$ and $K_{r,CEMO}$ vs. $\bar{t}_c$

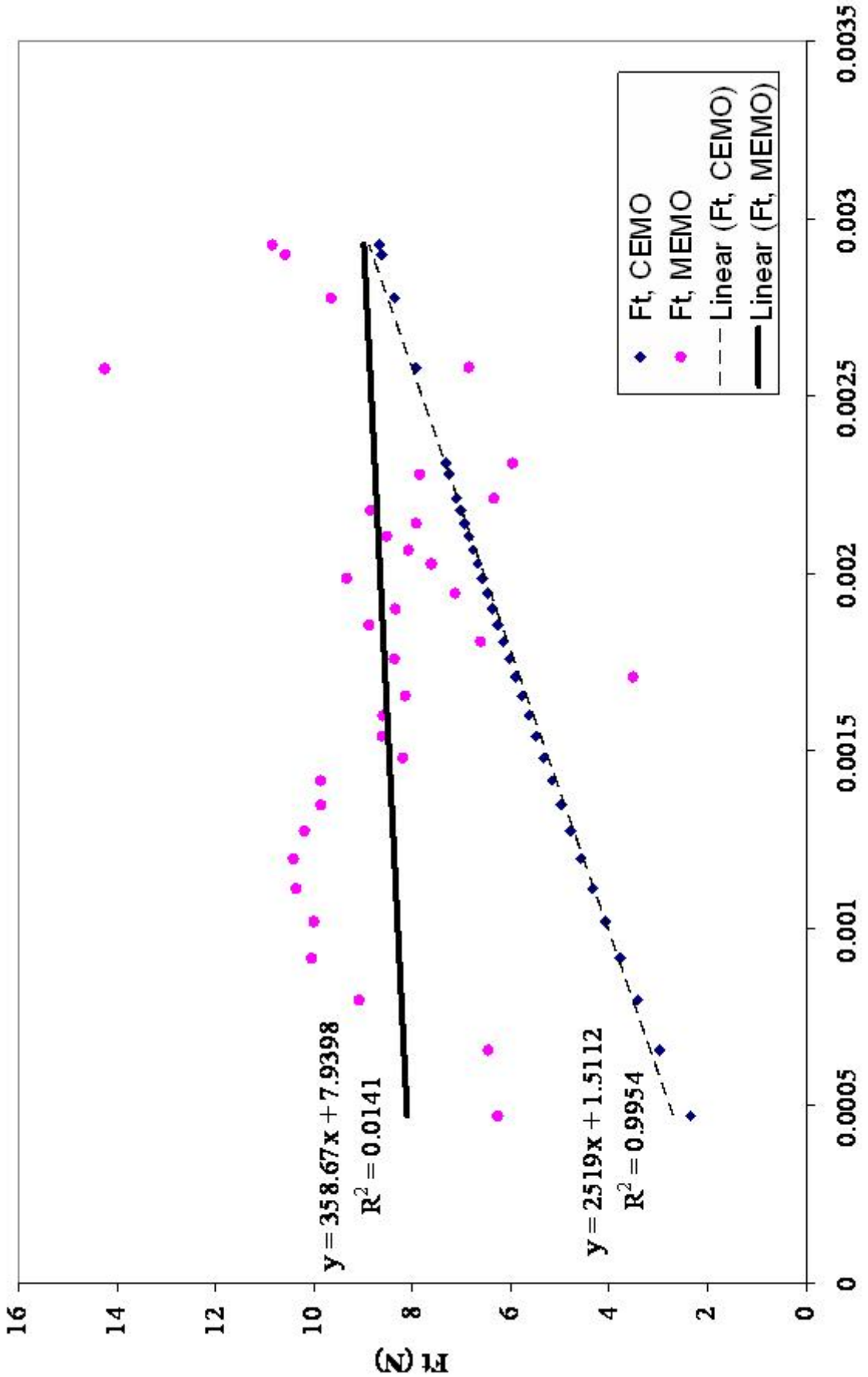

Figure 13: Comparison of $F_{t,MEMO}$ and $F_{t,CEMO}$ vs. $\bar{t}_c$

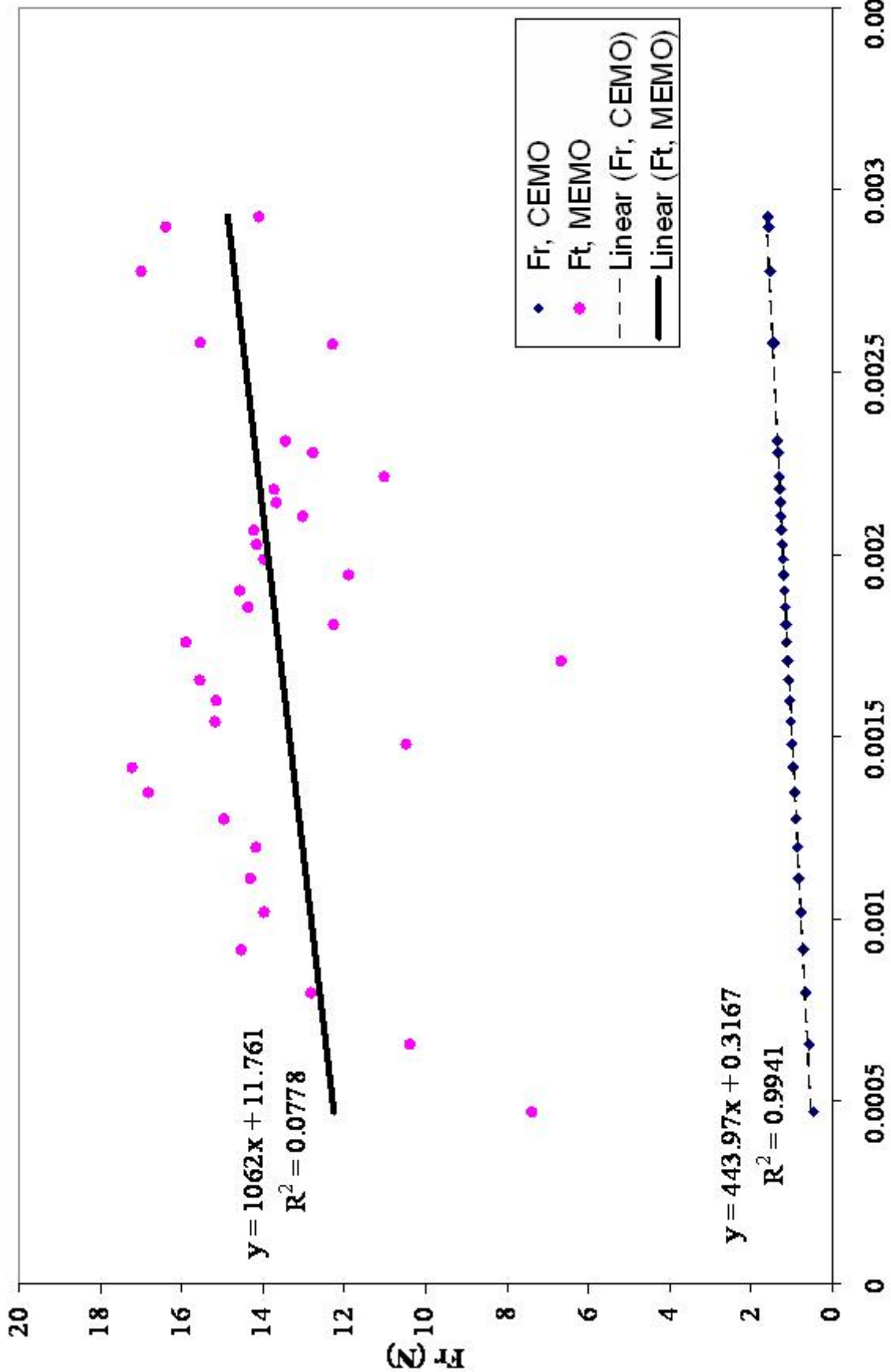

Figure 14: Comparison of $F_{r,MEMO}$ and $F_{r,CEMO}$ vs. $\bar{t}_c$

REFERENCES

[1] "Hardinge resumes production of classic bridgeport milling machines - scanning the horizon," *Modern Machine Shop*, June 2003. http://www.findarticles.com/p/articles/mi_m3101/is_1_76/ai_102947918.

[2] Armarego, E. J. A. and Deshpande, N. P., "Computerized end-milling force prediction with cutting models allowing for eccentricity and cutter deflections," *CIRP Annals*, vol. 40, 1991.

[3] Bao, W. Y. and Tansel, I. N., "Modeling micro-end-milling operations. part i: analytical cutting force model," *International Journal of Machine Tools and Manufacture*, vol. 40, pp. 2155–2173, 2000.

[4] Bao, W. Y. and Tansel, I. N., "Modeling micro-end-milling operations. part ii: tool run-out," *International Journal of Machine Tools and Manufacture*, vol. 40, pp. 2175–2192, 2000.

[5] Bao, W. Y. and Tansel, I. N., "Modeling micro-end-milling operations. part iii: influence of tool wear," *International Journal of Machine Tools and Manufacture*, vol. 40, pp. 2193–2211, 2000.

[6] Ber, A. and Feldman, D., "A mathematical model of the radial and axial throw of square indexable inserts in face milling cutter," *CIRP Annals*, vol. 26, p. 19, 1976.

[7] Ber, A. and Feldman, D., "The influence of radial location on the wear behavior of multi-tooth face milling," *CIRP Annals*, vol. 26, p. 1, 1977.

[8] Budak, E. and Altintas, Y., "Prediction of milling force coefficients from orthogonal cutting data," *ASME Manufacturing Science and Engineering*, vol. 64, p. 453, 1993.

[9] Chuzhoy, L. and DeVor, R. E., "Machining simulation of ductile iron and its constituents, part 2: Numerical simulation and experimental validation of machining," *ASME Journal of Manufacturing Science and Engineering*, vol. 125, pp. 192–201, 2003.

[10] Chuzhoy, L., DeVor, R. E., Kapoor, S. G., Beaudoin, A. J., and Bammann, D. J., "Machining simulation of ductile iron and its constituents, part 1: Estimation of material model parameters and their validation," *ASME Journal of Manufacturing Science and Engineering*, vol. 125, pp. 181–191, 2003.

[11] Engin, S. and Altintas, Y., "Mechanics and dynamics of general milling cutters. part i: helical end mills," *International Journal of Machine Tools and Manufacture*, vol. 41, pp. 2195–2212, 2001.

[12] Engin, S. and Altintas, Y., "Mechanics and dynamics of general milling cutters. part ii: inserted cutters," *International Journal of Machine Tools and Manufacture*, vol. 41, pp. 2213–2231, 2001.

[13] Furukawa, Y. and Moronuki, N., "Effect of material properties on ultraprecise cutting processes," *Annals of the CIRP*, vol. 37, no. 1, pp. 113–116, 1988.

[14] Gu, F., Kapoor, S. G., DeVor, R. E., and Bandyopadhyay, P., "An approach to on-line cutter runout estimation in face milling," *Transactions of NAMRI/SME*, pp. 240–247, 1991.

[15] Hollingum, J., "Hexapods to take over?," *Industrial robot*, vol. 24, no. 6, pp. 428–431, 1997.

[16] Kim, C.-J., Mayor, J. R., and Ni, J., "A static model of chip formation in microscale machining," *Transactions of the ASME*, vol. 126, pp. 710–718, November 2004.

[17] Kline, W. A. and DeVor, R. E., "The effect of runout on cutting geometry and forces in end milling," *International Journal of Machine Tool Design and Research*, vol. 23, no. 2/3, pp. 123–140, 1983.

[18] Koenigsberger, F. and Sabberwal, A. J. P., "Chip section and cutting force during the milling operation," *CIRP Annals*, vol. 10, pp. 197–203, 1961.

[19] Koenigsberger, F. and Sabberwal, A. J. P., "An investigation into the cutting force pulsations during milling operations," *International Journal of Machine Tool Design and Research*, vol. 1, pp. 15–33, 1961.

[20] Koenigsberger, F. and Sabberwal, A. J. P., "An investigation into the cutting force pulsations during milling operations," *International Journal of Machine Tool Design*, vol. 1, p. 15, 1961.

[21] Kroneberg, M., *Machining Science and Application - Theory and Practice for Operation and Development of Machining Processes*. UK: Pergamon Press, first ed., 1966.

[22] Kussul, E. M., Rachkovskij, D. A., Baidyk, T. N., and Talayev, S. A., "Micromechanical engineering: A basis for the l0w-cost manufacturing for mechanical microdevices using microequipment," *Journal of Micromechanical Microengineering*, vol. 6, pp. 410–425, 1996.

[23] Li, H. Z., Liu, K., and Li, X. P., "A new method for determining the undeformed chip thickness in milling," *Journal of Materials Processing Technology*, vol. 113, pp. 378–384, 2001.

[24] Lu, Z. and Yoneyama, T., "Micro cutting in the micro lathe turning system," *International Journal of machine tools and manufacture*, vol. 39, pp. 1171–1183, 1999.

[25] Martellotti, M. E., "An analysis of the milling process," *Trans. ASME*, vol. 63, pp. 677–700, 1941.

[26] Martellotti, M. E., "An analysis of the milling process, part-ii down milling," *Trans. ASME*, vol. 67, pp. 233–251, 1945.

[27] Masuzawa, T. and Tonshoff, H. K., "Three-dimensional micromachining by machine tools," *Annals of the CIRP*, vol. 46, pp. 621–628, 1997.

[28] Montoery, D. and Altintas, Y., "Mechanism of cutting force and surface generation in dynamic milling," *Journal of Engineering Industry*, vol. 113, p. 160, 1991.

[29] Moriwaki, T. and Okuda, K., "Machinability of copper in ultraprecision micro diamond cutting," *Annals of the CIRP*, vol. 38, no. 1, pp. 115–119, 1989.

[30] Oxley, P. L. B., "A strain hardening solution for the shear angle in orthogonal metal cutting," *International Journal of Mechanical Science*, vol. 3, p. 68, 1989.

[31] Sabberwal, A. J. P., "Cutting forces in down milling," *International Journal of Machine Tool Design Research*, vol. 2, p. 27, 1962.

[32] Spiewak, S. A., "Analytical modeling of cutting point trajectories in milling," *ASME Journal of Engineering for Industry*, vol. 116, pp. 440–448, 1994.

[33] Spiewak, S. A., "An improved model of the chip thickness in milling," *Ann. CIRP*, vol. 44, no. 1, pp. 39–42, 1995.

[34] Tansel, I., Rodriguez, O., Trujillo, M., Paz, E., and Li, W., "Micro-end-milling-i. wear and breakage," *International Journal of Machine Tools and Manufacture*, vol. 38, pp. 1419–1436, 1998.

[35] Tansel, I., Rodriguez, O., Trujillo, M., Paz, E., and Li, W., "Micro-end-milling-ii. extending tool life with a smart workpiece holder," *International Journal of Machine Tools and Manufacture*, vol. 38, pp. 1437–1448, 1998.

[36] Tansel, I., Rodriguez, O., Trujillo, M., Paz, E., and Li, W., "Micro-end-milling-iii. wear estimation and tool breakage detection using acoustic emission signals," *International Journal of Machine Tools and Manufacture*, vol. 38, pp. 1449–1466, 1998.

[37] Tlusty, J. and Macneil, P., "Dynamics of cutting forces in end milling," *Annals of the CIRP*, vol. 24, no. 1, pp. 21–25, 1975.

[38] Vasile, M. J., Friedrich, C. R., Kikkeri, B., and Mcelhannon, R., "Micrometer-scale machining: Tool fabrication and initial results," *Precision Engineering*, vol. 19, pp. 180–186, 1996.

[39] Volger, M. P., DeVor, R. E., and Kapoor, S. G., "On the modeling and analysis of machining performance in micro-end-milling, part i: surface generation," *Transactions of the ASME*, vol. 126, pp. 685–694, November 2004.

[40] Volger, M. P., DeVor, R. E., and Kapoor, S. G., "On the modeling and analysis of machining performance in micro-endmilling, part i: cutting force prediction," *Transactions of the ASME*, vol. 126, pp. 695–705, November 2004.

[41] Wang, J.-J. J., *Convolution Modeling of Milling Force System and its Application to Cutter Runout Identification.* PhD dissertation, The Georgia Institute of Technology, Department of Mechanical Engineering, Apr. 1992.

[42] Wu, D. W., "A new approach of formulating the transfer function for dynamic cutting processes," *Journal of Engineering Industry*, vol. 111, p. 37, 1989.

[43] You, S. J. and Ehmann, K. F., "Scallop removal in die milling by tertiary cutter motion," *ASME Journal of Engineering for Industry*, vol. 111, pp. 213–210, 1989.

[44] You, S. J. and Ehmann, K. F., "Synthesis and generation of surfaces milled by ball nose and end mills under tertiary cutter motion," *ASME Journal of Engineering for Industry*, vol. 113, pp. 17–24, 1991.

[45] Yucesan, G. and Altintas, Y., "Improved modeling of cutting force coefficients in peripheral milling," *Journal of Machine Tool and Manufacture*, vol. 34, p. 473, 1994.

[46] Zhou, R. Z. and Wang, K. K., "Modeling of cutting force pulsation in face milling," *Annals CIRP*, vol. 32, no. 1, p. 21.